

NRE4232/6401

FINAL DESIGN REPORT

**ADVANCES IN THE SUB-CRITICAL, GAS-COOLED,
FAST TRANSMUTATION REACTOR CONCEPT**

W. M. Stacey, K. A. Boakye, S. K. Brashear, A. C. Bryson, K. A. Burns, E. J. Bruch, S. A. Chandler, O. M. Chen, S. S. Chiu, J-P. Floyd, C. J. Fong, S. P. Hamilton, P. B. Johnson, S. M. Jones, M. Kato, B. A. MacLaren, R. P. Manger, B. L. Merriweather, C. Mitra, K. R. Riggs, B. H. Shrader, J. C. Schulz, C. M. Sommer, T. S. Sumner, J. S. Wagner, J. B. Weathers, C. P. Wells, F. H. Willis, Z. W. Friis, J. I. Marquez-Danian, R. W. Johnson, C. de Oliveira, H. K. Park, and D. W. Tedder

*Nuclear & Radiological Engineering Program
Georgia Institute of Technology
Atlanta, GA 30332-0425
May, 2006*

Keywords: *transmutation, fast reactor, closing fuel cycle*

ABSTRACT

The design concept for a sub-critical, He-cooled, fast reactor, fueled with transuranics from spent nuclear fuel in coated TRISO particles and driven by a tokamak D-T fusion neutron source, is being developed at Georgia Tech. This paper reports 1) advances in the design concept intended to enable achievement of “deep-burn” of the transuranics and passive safety, 2) investigations of the possibility of reprocessing the TRISO TRU fuel and of extending the strength of the fusion neutron source, 3) more extensive analyses to confirm and improve the design with respect to the adequacy of the fuel and nuclear performance, heat removal, tritium self-sufficiency and shielding, 4) more extensive analyses to confirm that the ITER divertor, magnet and heating/current drive systems can be adapted, and 5) fuel cycle analyses to further investigate the contribution that such a reactor could make to closing the nuclear fuel cycle.

I. INTRODUCTION

A concept for a sub-critical, fast reactor that would be fueled with transuranics (TRU) from spent nuclear fuel (SNF) is being developed at Georgia Tech. Previous conceptual design studies¹⁻⁵ and fuel cycle analyses^{6,7} have established a preliminary design concept for an annular sub-critical fast reactor surrounding a tokamak fusion neutron source. The original studies^{1,2,5,6} were for reactors fueled with pure TRU in a metal form and cooled with liquid lithium, while the recent studies³⁻⁵ were for reactors fueled with pure TRU in coated particle form and cooled with He.

Passive safety against a Loss-of-Coolant Accident (LOCA) and achievement of “deep burn” (>90% TRU fissioned) in coated particle (TRISO) pure TRU fuel with minimal reprocessing have been goals of the latter series of Gas Cooled Fast Transmutation Reactor (GCFTR) studies. Previous analysis⁴ identified the requirement for emergency core coolant in order for the GCFTR to survive a LOCA. Thus, one of the major purposes of this follow-on design study was to re-examine the requirement for an Emergency Core Cooling System (ECCS) and to develop the design concept for a passively activated accumulator ECCS (section V).

The results of a follow-on fuel cycle analysis⁷ indicate that the GCFTR-2 could meet the >90% TRU burnup objective with repeated recycling (about 15% TRU burnup per 5-batch burn cycle) with reprocessing to remove fission products and replenish depleted TRU. The results of this study suggested that in order to achieve the objectives of deep burn of TRU without reprocessing, the design of the GCFTR should be changed to either 1) allow for a stronger neutron source to compensate a greater negative reactivity accumulation [$P_{fis} \leq \ell P_{fus} / (1 - k_{eff})$], or 2) admix ²³⁸U with the TRU fuel to produce fresh TRU fuel in situ to offset the negative reactivity decrement of TRU depletion and fission product buildup, or both. The second option would be inconsistent with a purely deep-burn transmutation goal for GCFTR, but would be consistent with the somewhat broader goal of more effective utilization of the uranium mined for nuclear fuel (including extraction of energy from the TRU in SNF).

Investigations of these two options for achieving deep burnup without reprocessing are also major purposes of this follow-on design study. The practical upper limit on fusion power (neutron source strength) for a tokamak of the dimensions of the

GCFTR-2³ neutron source (major radius 3.7 m, minor radius 1.1m) operating within the ITER design database⁸ was evaluated, in order to determine the allowable increase of fusion neutron source strength that is available to compensate the reactivity decrease due to fission product buildup and TRU depletion in the fuel kernels (section VI). A redesign of the TRISO fuel particle to maximize the lifetime against fission product gas buildup was carried out, and the fuel pin clad radiation damage lifetime was evaluated for the previous reference zircaloy and other clad materials (section III). The consequences of admixing ²³⁸U with TRU within the TRISO fuel kernels to produce additional TRU to reduce the reactivity decrease due to fission product buildup and TRU depletion was also evaluated (sections IV and VII).

Since the follow-on fuel cycle analysis⁷ indicated that, with repeated recycling with reprocessing, the previous GCFTR-2 design could achieve > 90% TRU burnup with fusion neutron sources in the range $P_{\text{fus}} < 200$ MW, another major purpose of this follow-on design study was to examine the feasibility of reprocessing the TRISO TRU fuel particles to remove fission products and add fresh TRU in re-fabricated TRISO fuel particles (section III).

The core and neutron source designs and supporting analyses were extended in several respects. The neutron source heating and current drive system was defined (section VI) and the requirement for port access through the shield and reactor into the plasma was taken into account. The core nuclear and thermal analyses, the shielding design and analysis, and the tritium production design and analysis were extended and refined (sections IV and V). The fusion neutron source engineering design analysis was extended to evaluate the heat removal capability of the ITER divertor adaptation when the coolant was changed from water to helium and to confirm the structural aspects of the adaptation of the ITER toroidal field coil system (section VI).

II DESIGN OVERVIEW

A Configuration, Dimensions, Materials and Major Parameters

The GCFTR-2 reactor concept³ was the starting point for the analyses described in this paper. This reactor is a sub-critical, fast, helium cooled reactor driven by a tokamak D-T fusion neutron source. The configuration, overall dimensions, magnetic

field, and He coolant remained the same for GCFTR-3, but an increase in the plasma current to achieve a larger neutron source rate, changes of some fuel materials, definition of the heating & current drive and emergency core cooling systems, and other changes were sufficient to designate a new GCFTR-3 design. A 3-D depiction of the GCFTR-3 is shown in Fig. 1. The annular reactor surrounds the fusion plasma neutron source on the outboard side, and both are surrounded by a combination reflector and lithium-oxide blanket for tritium production and then by a shield. (A divertor below the plasma and an accumulator for emergency core cooling above the core are not shown.)

The detailed radial dimensions are indicated (but not all shown) in Fig. 1. The inner radius of the reactor core is 485 cm, the core width is 112 cm (100 cm fuel region) and the core height is 300 cm. The tokamak fusion neutron annular plasma source is on the inboard side of the reactor, with a width of 216 cm and a height of 367 cm. A divertor is located on the bottom inboard side of the plasma chamber. The plasma chamber and divertor are scaled down from the ITER (International Tokamak Experimental Reactor⁸) design. A 3.5 cm thick first wall of the plasma chamber separates the core and plasma regions. Both the plasma and the reactor core are surrounded by a blanket-shield which is 79.5 cm thick, which in turn is surrounded by a 6 cm thick vacuum vessel. This entire annular configuration--reactor, plasma, blanket, shield, vacuum vessel--is contained within a ring of 16 “D-shaped” superconducting toroidal field coils, each of radial thickness 43 cm and toroidal thickness 36 cm. The vacuum vessel abuts the toroidal field coils on the inboard side. Just inside the toroidal field magnets is the central solenoidal magnet of thickness 48 cm. The remaining “flux core” space inside the central solenoid has a radius of 88 cm.

B. Major Parameters and Materials

Table 1 gives the major parameters and materials used in the GCFTR-3. The parameters and materials were designed for a TRISO fuel particle that has a TRU-U-oxide kernel that is surrounded by SiC, WC and ZrC layers, which are embedded in a SiC matrix. All structural materials are oxygen dispersion strengthened (ODS) martensitic steel.

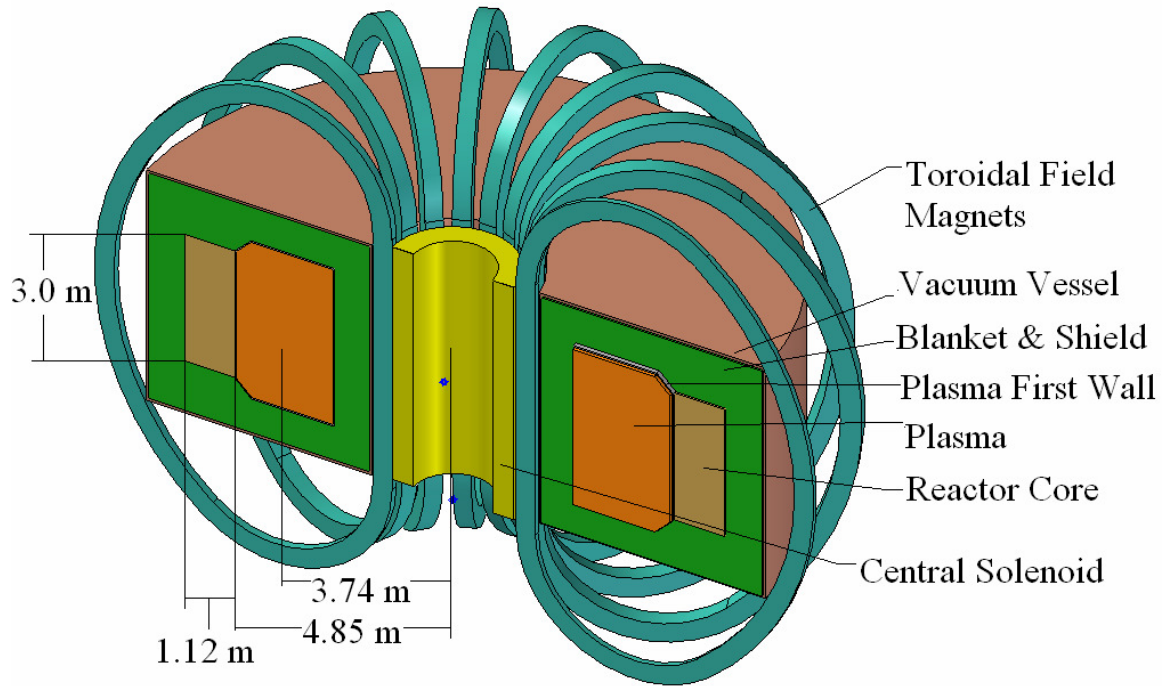


Figure 1. Configuration of the GCFTR-3.

Table 1. Major Parameters and Materials of the GCFTR-2

Parameters and Materials	Values
Reactor	
Annular dimensions	$R_{in} = 4.85 \text{ m}$, $R_{out} = 5.97 \text{ m}$, $H = 3 \text{ m}$
Fuel/He/structure v/o	60/30/10
Fuel element	TRISO particles in SiC matrix, pins $d = 1.34 \text{ cm}$
TRU-U coated particle diameter	$660 \mu\text{m}$
TRU-U-oxide fuel packing factor	62%
TRU-U fuel mass	74 MT
Maximum k_{eff}	0.95
He mass flow , He temperature	$M = 3280 \text{ kg/s}$, $T_{He}^{in}/T_{He}^{out} = 280/494 \text{ }^\circ\text{C}$
Power density, Maximum T_{fuel}	$q''' = 42.2 \text{ MW/m}^3$, $T_{fuel}^{max} = 669 \text{ }^\circ\text{C}$
Clad/structural materials	ODS martensitic steel
Fission Power	3000 MW_{th}
Blanket-Shield	
Shield Materials	ODS steel, He, B_4C , HfC, Ir, WC, Cd
Tritium Breeder	Li_2O
Thickness	79.5 cm
Tritium Breeding Ratio	1.1
Plasma	
Plasma current	$\leq 8\text{-}10.0 \text{ MA}$

Fusion power/neutron source rate	(50-500 MW)/(1.8e19 s ⁻¹ to 1.8e20 s ⁻¹)
Fusion gain ($Q_p = P_{fus}/P_{plasma\ heating}$)	3.2-5.1
<i>Superconducting Magnets</i>	
Field CS, TFC, on center of plasma	13.5 T, 11.8 T, 5.9 T
<i>Divertor</i>	
Materials	W tiles on CuCrZr, He cooled
Heat flux	≤ 2.0 MW/m ²
<i>First Wall</i>	
Materials	Be on ODS, He cooled
Neutron wall load (14 MeV)	≤ 1.8 MW/m ²
Heat flux	≤ 0.4 MW/m ²

C. Component Radiation Damage Lifetime

Fuel lifetime against radiation damage is crucial for the achievement of the TRU burnup objectives of GCFTR-3. In the reprocessing option, in which deep burnup is achieved by repeated 8.2 yr, 5-batch burns that each achieve 25% TRU burnup, the minimum requirement is survival of the fuel for a fast (>0.1 MeV) neutron fluence of 6.9×10^{22} n/cm². In the non-reprocessing option, in which deep burnup is achieved in a single 33.9 yr, 5-batch burn that achieves 94% TRU burnup, the requirement is survival of the fuel for a fast (>0.1 MeV) neutron fluence of 4.3×10^{23} n/cm².

Unfortunately, there is little data for TRISO particles at deep burnup. The Peachbottom Reactor irradiated TRISO particles with a fast fluence of 1.3×10^{21} n/cm² at temperatures 800-1350°C, with a failure rate of 1.4×10^{-6} (Ref. 9). More recent results from development programs in the US and Germany have achieved burnups as large as 80% FIMA and fast neutron fluences as large as 1.2×10^{22} n/cm² with failure rates of 10^{-4} to 10^{-6} for the higher FIMA US tests and 10^{-7} to 10^{-9} for the order 10% FIMA German tests¹⁰. Achievement of the fluence lifetimes required for a deep burn transmutation reactor like GCFTR-3 is a major challenge for TRISO fuel development.

The fuel cladding and fuel assembly structure lifetimes against radiation damage are also important considerations. The minimal requirement for the ODS clad is to survive the 5-batch residence time of 8.2 years for the reprocessing option, which corresponds to a fast neutron fluence of 6.9×10^{22} n/cm². The maximum requirement for the ODS clad is to survive the single 5-batch residence time of 32.9 years for the non-reprocessing option, which corresponds to a fast neutron fluence of 4.3×10^{23} n/cm².

Lifetime of the ODS martensitic steel structure can only be estimated; using the values of 80-150 dpa quoted for HT-9¹¹ corresponds to $1.5-3.0 \times 10^{23}$ n/cm² fast neutron fluence.

The plasma chamber “first wall”, which consists of 3 cm of ODS martensitic steel, would receive a fast neutron fluence of 7.5×10^{23} n/cm² over 30 effective full power years (EFPY) of operation. Using the same estimate for the radiation damage lifetime of ferritic steel as above, this would require 2-4 first wall replacements.

The shield was designed to protect the superconducting magnets from radiation damage failure over a 30 EFPY lifetime.

The ITER divertor⁸, after which the GCFTR-3 divertor is modeled, is expected to require replacement 8 times during ITER lifetime because of plasma erosion of the surface. The plasma flux to the divertor in ITER is a few times greater than in GCFTR-3, but the GCFTR-3 lifetime is several times longer than that of ITER, so that tens of divertor replacements might be anticipated for GCFTR-3.

The radiation damage lifetime estimates are summarized in Table 3.

Table 2. Component Radiation Damage Lifetimes

Component	GCFTR-3 fast neutron fluence (n/cm ² >0.1MeV)	LIMIT fast neutron fluence (n/cm ² >0.1MeV)
<i>Reactor</i>		
Clad		
8.2 yr, 25% TRU burnup	6.9×10^{22}	$1.5-3.0 \times 10^{23}$ ^a ?
32.9yr, 94% TRU burnup	4.3×10^{23}	$1.5-3.0 \times 10^{23}$ ^a ?
TRISO Fuel particle		
8.2 yr, 25% TRU burnup	6.9×10^{22}	?
32.9yr, 94% TRU burnup	4.3×10^{23}	?
<i>Fusion Neutron Source</i>		
TFC Nb ₃ Sn 30 EFPY	1.6×10^{18}	1×10^{19} ^b
TFC insulation 30EFPY	3.1×10^7 rad	10^9-10^{10} rad ^b
First-wall 30EFPY	7.5×10^{23}	$1.5-3.0 \times 10^{23}$ ^a ?
Divertor		Plasma erosion

^a Ref. 11, ^b Ref. 12

III FUELS

1. The Fuel Kernel and TRISO Particle

The TRISO fuel particle was selected over the BISO since the TRISO's additional layer provides more structural support. This reduces the actual fuel capacity within the reactor but provides a more stable particle, which is desirable from a lifetime standpoint.

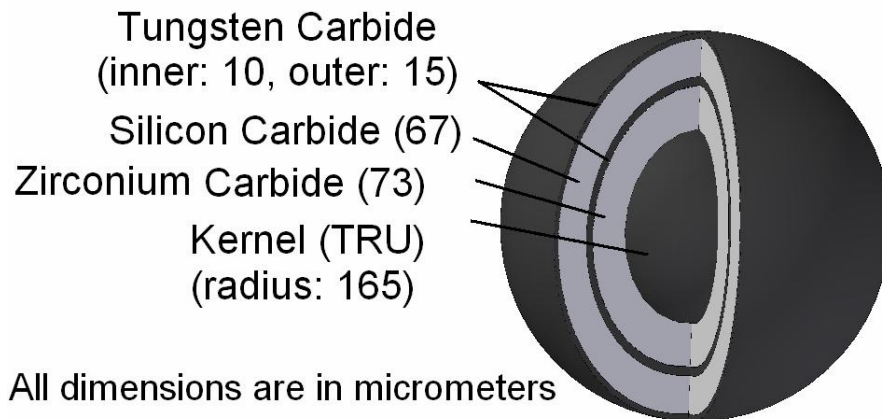


Figure 2: TRISO Particle

With respect to Fig. 2, the particle consists of a center fuel kernel surrounded by a ZrC buffer and three supporting layers. The buffer absorbs fission gases and serves to stop recoil fission products. The innermost WC layer serves as a shield to protect the kernel from chlorine, which is used in the fabrication process in bonding the subsequent coatings. The SiC layer is the primary structural component, and the outer WC layer provides an extra layer of protection.

For survival in a fast reactor, it was necessary to modify the conventional TRISO particle, which was developed for thermal reactors. In thermal reactors, pyrolytic carbon has been used to form both the inner and outermost coatings after the buffer. Unfortunately, pyrolytic carbon contracts under irradiation at a rate proportional to neutron energy; therefore, the inner layer may contract too quickly in a fast flux and become unattached to the next layer. This results in cracking and failure of the particle¹³. WC has an ultimate tensile stress of 344 MPa and a high modulus of elasticity, which make it a possible replacement for pyrolytic carbon, which has a lower ultimate tensile stress of approximately 160 MPa. The melting temperature of WC, 2780°C, is well above the peak temperature calculated for the LOCA scenario with a passively activated

emergency core cooling system (section V), which implies a significant margin between the WC melting temperature and any anticipated peak fuel temperature. The layer after the buffer consists of silicon carbide, which provides the primary structural support for the particle. Zirconium carbide with 50% porosity has been chosen for the buffer layer since a material with a high affinity to oxygen is needed⁴ to control the buildup of oxygen-based gases.

The particles receive an intense amount of high-energy neutron radiation during their lifespan, which may cause swelling and cracking¹⁴. Extensive research on TRISO particles in both fast and thermal fluxes has been done, indicating that these failure mechanisms are of concern only when large temperature gradients in individual particles or particle irregularities outside of manufacturing specifications occur.^{14,15} Because of the inability to obtain pertinent data regarding these failure mechanisms for the designed particle, only pressure buildup due to gaseous fission products inside the particle was examined quantitatively.

With a fuel consisting initially of 70% TRU-oxides and 30% ²³⁸U, ORIGEN¹⁶ predicted a 73% reduction of the amount of TRU in the kernel after 30,000 days. Predicted fission gas concentrations for up to 30,000 days operation were used to calculate the pressure within the particle and projected linearly to predict pressures at 90% burnup. Helium, krypton, iodine, xenon, and bromine gases were the main contributors to pressure buildup⁴. At the nominal maximum fuel centerline operating temperature of 942 K (section V), it was assumed that the gases could be modeled as ideal. Because the silicon carbide layer is the dominant structural layer in the particle and has a radius less than 10% of the total kernel radius, the stress in the particle wall could be calculated using expressions for a thin-walled pressure vessel (Appendix A). The particle size was optimized using the assumptions above, and keeping the sum of the thicknesses of the buffer and SiC layers constant. A slight reduction was taken from the optimized buffer radius in order to preserve the assumption of a thin-walled pressure vessel. The inner layer, which serves as a chemical shield during the fabrication process, is bonded to the second layer, and because it provides little structural support, it is ignored in the initial optimization¹⁷. The kernel diameter was set to 330 μm to

accommodate the core fuel density necessary for adequate neutron multiplication. The final layer dimensions and material properties are given in Table 3.

Using these dimensions, the pressure in the buffer was calculated at various burnups. Pressure and stress in each layer are plotted versus burnup in Figure 3. The interior pressure increased linearly to 44.4 MPa at 90% burnup, and this pressure creates a stress of 85.4 MPa on the SiC layer.

Table 3: TRISO Particle Dimensions and Properties

	Thickness (μm)	Ultimate Tensile Stress (MPa)	Young's Modulus (GPa)	Poisson's Ratio	Density (g/cm ³)
Kernel	(radius) 165				
Buffer	73				
Inner WC	10	344	668	0.24	15.8
SiC	67	200	410	0.14	6.73
Outer WC	15	344	668	0.24	15.8

* Silicon Carbide was noted by NIST as having $\sigma_{UTS} = 200$ MPa. Other values have been noted, but this takes the most conservative approach.

The outer layer is not susceptible to failure due to gas pressure, but expansion of the silicon carbide layer is of concern. Calculations using Young's Modulus and Poisson's Ratio were used to determine the amount of stress in the outer layer due to interior expansion (Appendix A). At 90% burnup, the WC will have a stress of 157.4 MPa applied to its inner wall. Pressure and stress in each layer are plotted versus burnup in Fig. 3. Due to the large differences between the ultimate tensile strengths of the layer materials and the stresses expected to be placed on the layers, it is not anticipated that the particle will fail due to fission product gas pressure buildup. For the same reason, the particle can withstand a temperature transient up to 1318 K, a reduction in ultimate tensile strength by 57%, or a decrease in either the buffer or SiC layer which would allow a higher fuel density. Because SiC hardens with irradiation, an additional measure of conservatism is inherent in these calculations.¹⁸

Radiation damage remains an essential concern in determining the lifetime of the particle, but more research will be needed before the subject can be further explored. In addition to material changes and transmutation gas buildup due to (n,p) and (n, α) reactions in all components due to neutron irradiation, shear stress between the coating

layers of the particle may cause cracking which could lead to particle failure.¹⁹ Kernel migration in the buffer and associated hot spots also require further work. It may be possible to change material of the buffer to decrease kernel shifting, so long as a material with an affinity for oxygen and porosity is used. Additionally, WC is a new material for this application, and additional research into it is needed.

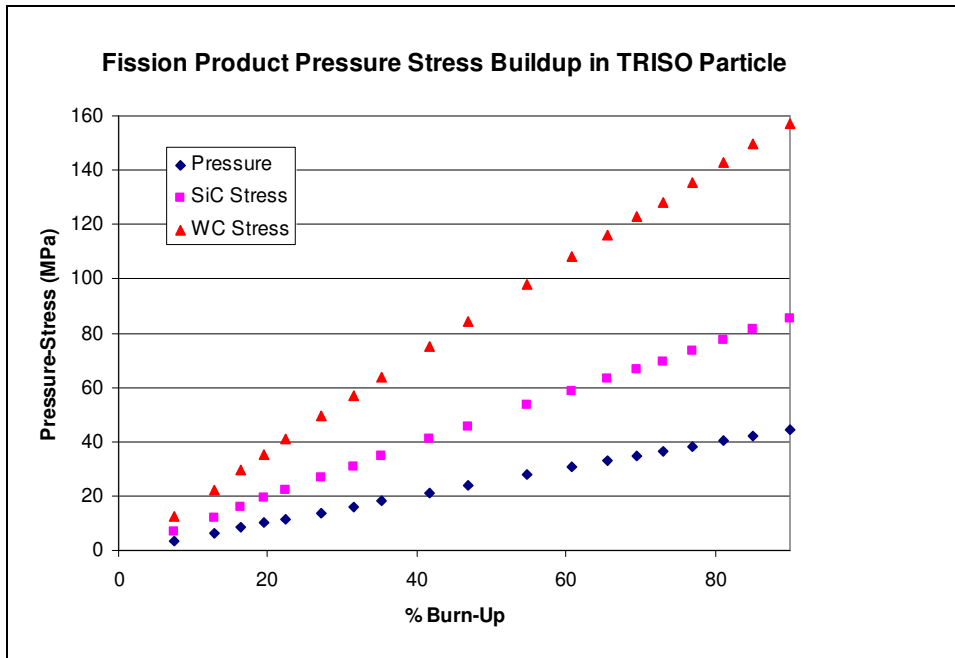


Figure 3: Pressure and Stress versus Burnup

2. Cladding

The cladding for the GCFTR-2 design was Zircaloy-4 alloy³. A major problem with Zircaloy, however, is that it expands extensively in a fast neutron spectrum¹⁴. This would make fuel pin design very difficult, and therefore determination of a more promising clad material was an objective of this study. Two materials that were strongly considered for cladding for this reactor design were ODS martensitic steel and SiC, the properties of which are given in Table 4.

As shown in Table 5, 1DS steel, a typical ODS, has a similar composition to HT-9, a typical ferritic/martensitic steel, but has differences due to the addition of Y_2O_3 particles. HT-9 has been widely used in fast reactors in the past because, unlike austenitic steels, it has excellent swelling resistance. The ODS steel retains these excellent swelling

resistance properties²⁰ (Appendix A). The small Y₂O₃ precipitates (<20 nm) present in ODS steel serve two major purposes. First, they stabilize the matrix by blocking mobile dislocations. Second, they act as a sink of radiation induced point defects²¹. This allows the ODS steels to be more stable at higher operating temperatures while maintaining reasonably similar mechanical and thermal properties to HT-9.

There are several drawbacks to ODS steel. The melting temperature, 1400-1500 K, falls short of the clad temperature calculated in LOCA analyses of GCFTR without emergency core cooling (section V). Early ODS steels had trouble with anisotropy in mechanical properties. However, recent developments in the heat treatment process have alleviated this problem²². The hardness of the material initially caused some complications in processing, but this problem has also been solved²¹. In addition, ODS steel has marginal oxidation resistance at high temperatures²³.

SiC has several advantages that make it an excellent candidate for cladding in high-temperature fast reactors. It has an extremely high melting point (~3400 °C), very high strength (UTS ~200 MPa), and low swelling(~1%).¹⁸ Brittleness is an issue with pure SiC, but fracture toughness of SiC fibers in a SiC matrix (25 MPa m^{1/2})²⁴ is nearly an order of magnitude higher than that of pure SiC (3.1 MPa m^{1/2})²⁵. Another issue that needs to be addressed in pure SiC is the thermal conductivity degeneration due to high temperature irradiation. However, certain SiC composites show a lesser decrease in thermal conductivity than pure SiC²⁴.

An oxide dispersion strengthened (ODS) martensitic steel was chosen for the reference cladding material. SiC was not chosen largely because of the lack of published data on its current use in fast reactors.

Table 4: Cladding Materials²³

	Operating Temp [K]	Melting Temp [K]	Main Disadvantage
Zircaloy-4	<2118	2118	Expands under fast flux; Low melting point
SiC	923-1223	3646	Brittle
Ferritic/martensitic steel	543-773	1400-1500	Low melting point
ODS martensitic steel	598-983	1400-1500	Low melting point

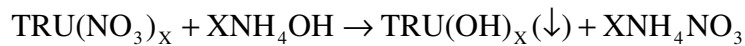
Table 5: Compositions (%) of ODS and HT9²⁶

Alloy	1DS	HT9
Fe	Balance	Balance

Cr	11.0	12.0
W	2.7	3 Mo
Ti	0.5	0.5
Ni	0.1	0.1
C	0.1	0.2
P	0.005	0.01
S	0.001	0.005
Free O	0.11	---
Y ₂ O ₃	0.6	n.a.

3. Fuel Fabrication

The TRISO fuel kernels will be fabricated using a sol-gel (solution-gelation) process. The transuranics (TRUs) coming from the UREX/TRUEX processes will be in a nitrate form. In order to change the nitrate into a hydroxide and ultimately an oxide, the following chemical reaction occurs in the mixer in Fig. 4:



where X depends on the valence state of the particular element being reacted. The sol is obtained by first mixing the TRU nitrate (TRU(NO₃)) with ammonium hydroxide (NH₄OH) and the resulting TRU hydroxide (TRU(OH)) precipitates out of solution. The ammonium nitrate is removed by stirring the solution and washing with water. Then, nitric acid (HNO₃) is added to the TRU hydroxide precipitate to form the final sol. In order to avoid the use of a gelation agent, the nitric acid/TRU ratio must be 0.6 or higher. The sol is then heated to 70°C for about three hours²⁷ and a surfactant is added in order to keep particles from sticking together²⁸.

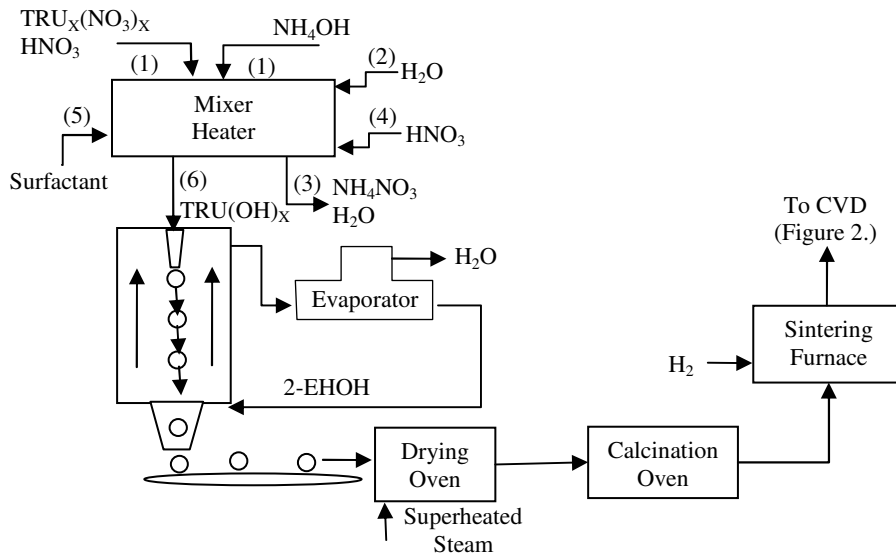


Figure 4: Kernel Fabrication

The gelation process takes place by forcing the sol through a very small needle into a liquid atmosphere of 2-ethyl-hexanol (2-EHOH). Surface tension forms the sol into droplets which are proportional in size to the diameter of the needle. Gravity forces the droplets downward against a countercurrent of 2-EHOH. 2-EHOH extracts the remaining water from the droplets left over from the sol stage. The 2-EHOH is contained in a separate loop and is run through an evaporator to remove the excess water and recycle the 2-EHOH. The kernel droplets are released from a nozzle one at a time onto a conveyor belt where the 2-EHOH is drained off²⁷.

The droplets are then dried in an atmosphere with superheated steam at 250°C for 10 minutes. Drying in an atmosphere of superheated steam allows for a more even drying from the inside of the kernel to the outside, which prevents cracking²⁸. The kernels are then sent through a calcination oven at 300°C in an air atmosphere. Lastly, the kernels are sintered in a reduction furnace in an atmosphere of H₂ at a temperature of 1600°C. This is where the fuel form can further be controlled. The H₂ combines with the oxygen in the fuel to form water. So, the more H₂ present in the atmosphere, the lower the oxygen content of the final fuel kernel¹⁰.

The TRISO particle's fabrication process is depicted in Fig. 5. The layers will be fabricated using chemical vapor deposition (CVD). This will be a continuous process,

similar to the German process¹⁰. CVD works on the principle of a temperature difference between the particle and the surrounding vapor, which consists of a mixture of argon and the gaseous material to be deposited. The particle, which is constantly rolling through the deposition oven, is at a relatively cooler temperature than the surrounding vapor. The vapor essentially condenses evenly on the particle, thereby forming that particular layer of the TRISO particle. Deposition rates typically vary between 4-10 $\mu\text{m}/\text{min}$, and the length of the deposition oven is dependent on how thick the desired layer must be and the deposition rate. There are also aging ovens in between each deposition stage in order to allow for the layer to cure and the particle to cool back down to a suitable temperature.

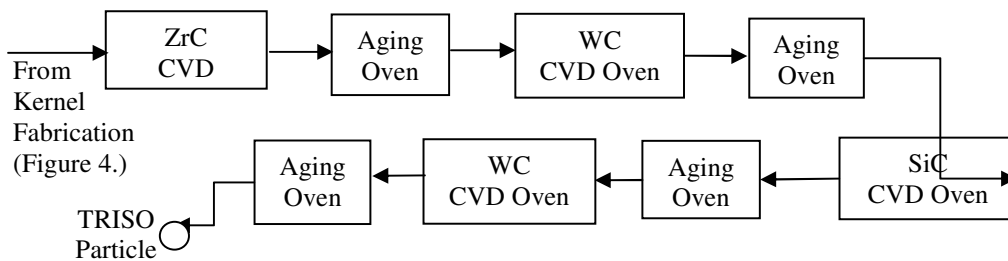
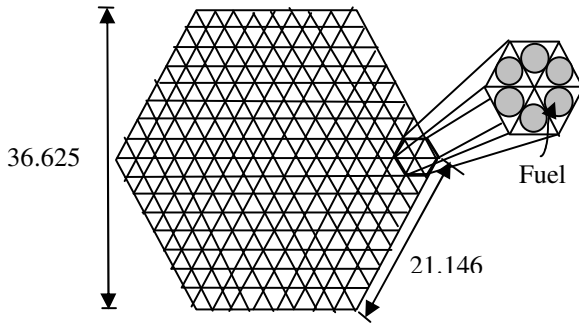


Figure 5: TRISO Particle Layer Fabrication

Once the TRISO particles are ready, fuel pellets will be fabricated. These are made using chemical vapor infiltration (CVI)³⁰. These cylindrical pellets consist of TRISO particles embedded in a SiC matrix. CVI is only useful for short distances due to potential blocking of the tubes as SiC travels through the packed TRISO particles. This limits the pellet to only two inches in length. A maximum packing factor for this geometry of 62% could theoretically be achieved. However, a realistic packing factor for this geometry is 50-60%³. These fuel pins are then stacked end-on-end and surrounded with a steel cladding and sealed on both ends.

Table 6. Fuel Pin Parameters

Flat to Flat Distance	36.625 cm
Side Length	21.146 cm
Assembly Height	300 cm
Pin Diameter w/clad	1.526 cm
Pins/assembly	384
Assemblies/core	245
Total pins in core	94080

**Figure 6: Fuel Assembly Cross Section**

The fuel assembly is hexagonal with a triangular grid (Fig. 6 and Table 6). There will also be a spacer grid mid-way up the assembly. The total number of assemblies in the core is 245. There are no half-assemblies due to the complication of fabricating half-assemblies.

The use of carbide fuels needs to be closely examined. Carbides may be superior to oxides due to the lower vapor pressure of AmC than AmO_x. Also, if carbides were used, there may be less of a need for the large ZrC oxygen-getter layer of the particle thereby allowing for a larger fuel kernel and a higher fuel v/o.

The use of a melt-casted metallic fuel pellet instead of TRISO particles³¹ should be examined.

4. Reprocessing

As discussed above, the designed fuel particle is expected to withstand fission product pressure buildup to high burnup, but radiation damage or the reactivity decrement associated with high burnup may make it necessary to remove the particles before 90% actinide burnup has been achieved. Thus, we investigated a possible reprocessing scheme which integrates the GCFTR fuel recycle with a LWR fuel reprocessing facility. The UREX/TRUEX series has been selected over the DIDPA process which was previously presented³ due to the buildup of degradation products in the DIDPA organic solvent limiting recycles. The CEREX and ALCOLEX process has been proven to be efficient in removing degradation products from the tributyl phosphate utilized as an organic solvent in UREX and TRUEX, allowing for sufficient recycle of the organic solvent. The modeled process is shown in Fig. 7.

All of the processes shown have been investigated and described in the literature, with the exception of the grinding of TRISO particles. Only the LWR Chop Leach and LWR UREX processes are necessarily commercial scale; the other processes are much smaller (hot cell) since actinides make up only about 1% of the spent fuel from the LWR and residence time in the GCFTR is significantly longer than that of a typical LWR. The proposed facility will utilize traditional “chop leach” head-end processes to separate the LWR fuel from the cladding. The separated LWR fuel will go into UREX to separate uranium for reuse or disposal; the UREX process has been demonstrated to achieve uranium extraction of greater than 99.99% on a lab scale³²⁻³⁴.

To accommodate the TRISO particle, the head-end process for the GCFTR fuel includes a grinding step to completely crush the particle into pieces no larger than 250 microns to ensure complete fuel kernel exposure for reprocessing. The two streams will be combined in the TRUEX step for recovery of transuranics (some of the remaining .01% uranium will co-extract). Following TRUEX, the extracted material will go through a final An/Ln separations process to remove remaining lanthanides from the TRU before going on to fuel fabrication. The TRUEX and An/Ln separations have been tested with greater than 99.8% recovery of TRU from high level liquid waste and fuel^{33,34}.

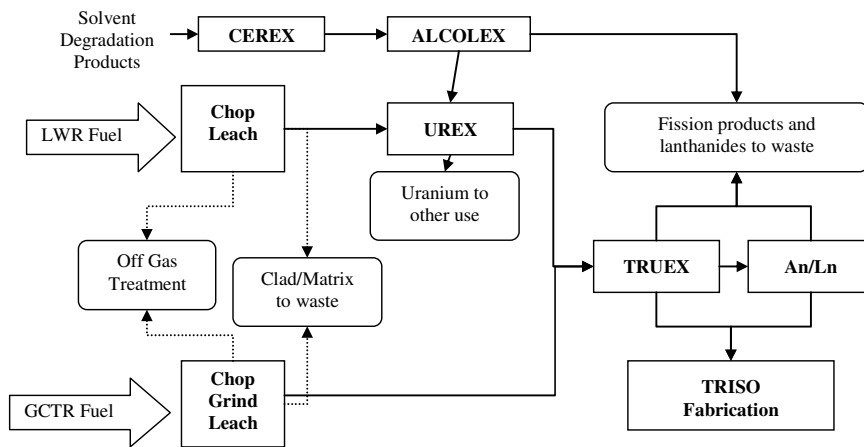


Figure 7: Proposed Combined LWR/GCFTR Fuel Recycle Processes

All of the steps associated with the GCFTR fuel require hot cell shielding for safety due to the increased radiological hazard presented by the buildup of certain

isotopes. While the changing nature of the fuel presents a challenge for operations, it also limits proliferation risk as the material is not considered weapons viable after a few recycles.

Further research into reprocessing is necessary to determine critical geometry, actual chemical material balance, and cost data. While reprocessing of TRISO particles is feasible, it is difficult due to the need for destruction of the TRISO particle and to significant waste material collection, and a less permanent fuel form is suggested if reprocessing is required.

IV. NUCLEAR

A. Nuclear Calculation Codes and Models

Horizontal and vertical cross section views of GCFTR-3 are given in Figs. 8 and 9. To model the core, the multidimensional multi-group spherical harmonics code EVENT³⁵ and the 3D continuous energy Monte Carlo codes MCNP³⁶ and KENO³⁷ were used. Both the MCNP and KENO models used the ENDF/B-V and ENDF/B-VI cross-section libraries. Two separate 2D (r-z and x-y) models were used. 3D EVENT and MCNP models that exactly represented the reactor core dimensions and compositions, including the two 20 degree core sectors at 180 degrees from each other devoted to heating and current drive ports (section VI), were also used. The 2D EVENT r-z model could not represent these 20 degree sectors, and the x-y EVENT model could not represent axial leakage but did represent the removed sectors. The EVENT models used 34 energy groups and a first order (P_1) spherical harmonic approximation for all calculations (except the shielding calculation). Cross-sections were acquired from an ISOTXS format library that had been generated from a FIDO file by a run of the TRANSX³⁸ program.

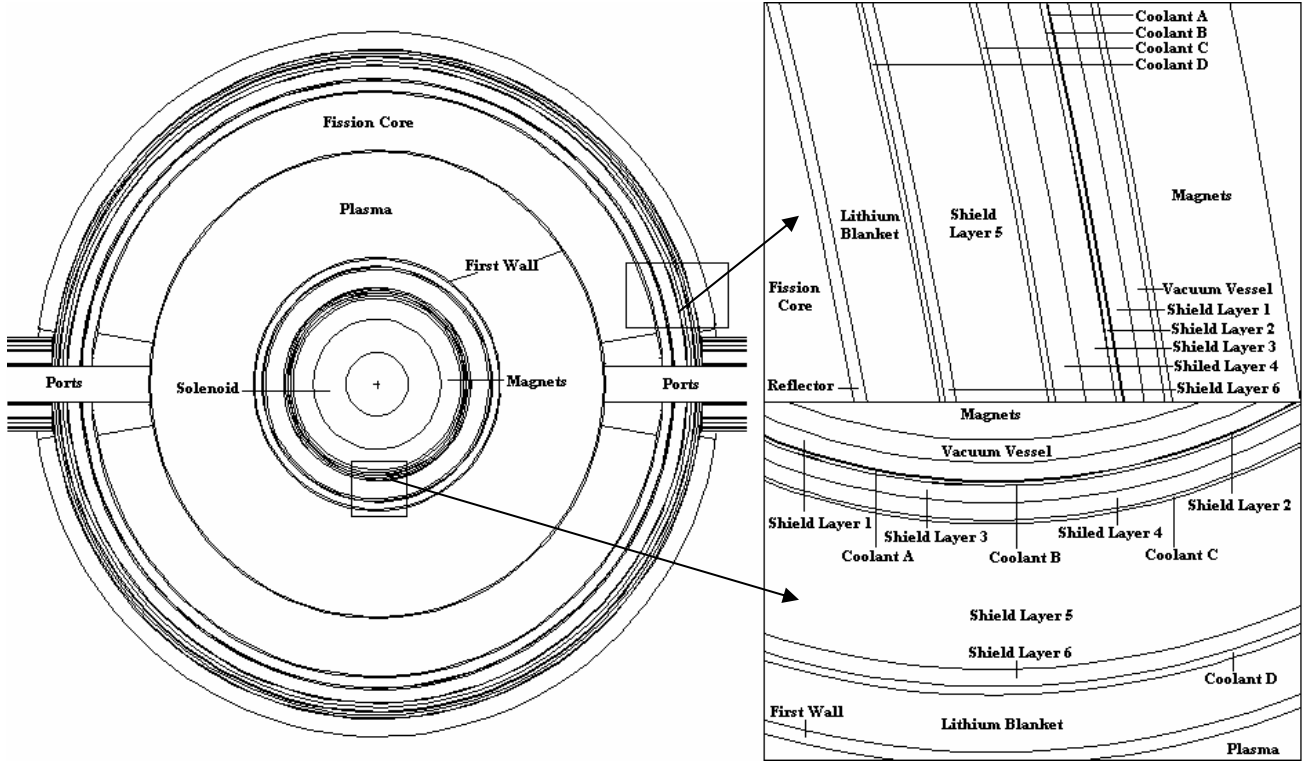


Figure 8: Horizontal Cross Sectional View of the GCFTR-3 Reactor

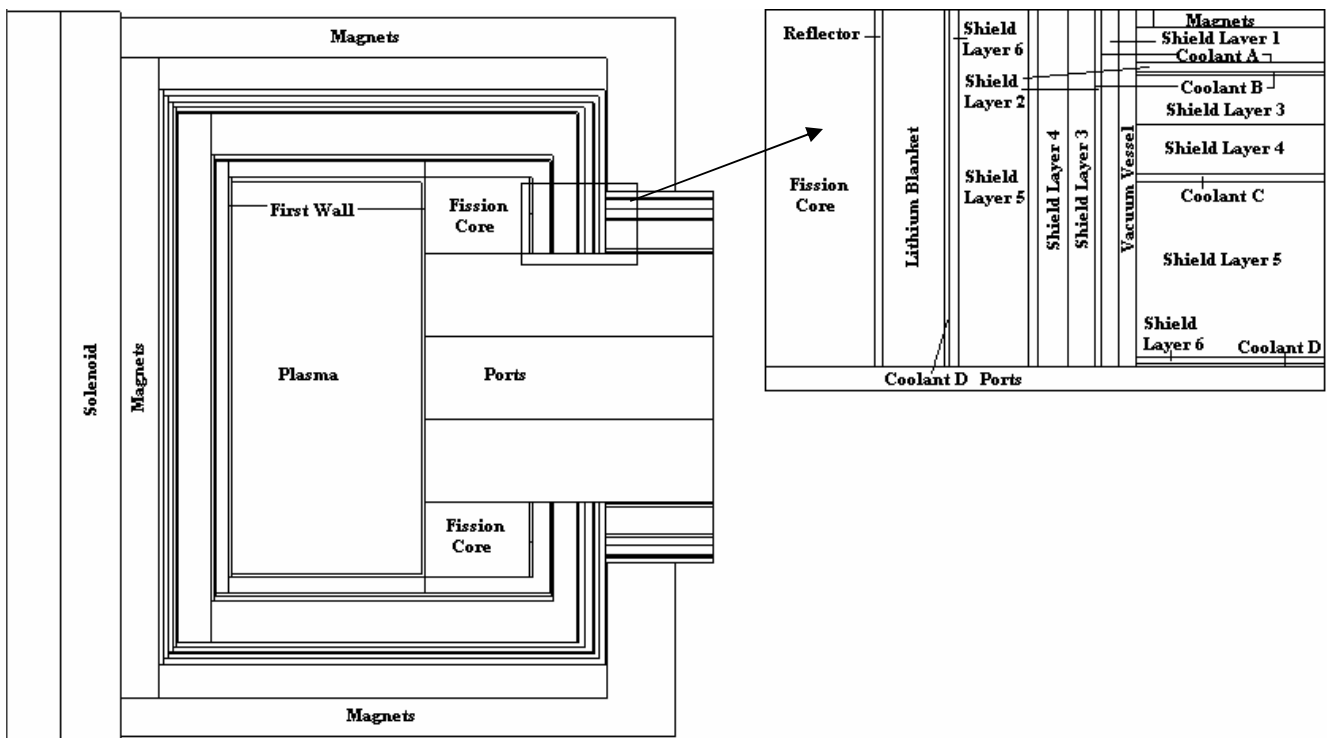


Figure 9: Vertical Cross-sectional views of the GCFTR-3 Reactor

B. Multiplication Constant

1. Range of Multiplication Constant

The primary goal of the Gas Cooled Fast Transmutation Reactor (GCFTR-3) is to achieve a deep burn of the transuranic actinides, while keeping k_{eff} below 0.95 yet above the minimum value that can be compensated by increasing the power of the fusion neutron source. This minimum value of k_{min} can be roughly estimated by recalling that the neutron population, which is proportional to the fission power, in a sub-critical reactor scales as $P_{\text{fis}} \propto \ell P_{\text{fus}} / (1 - k)$, where ℓ is the neutron lifetime and making use of the fact that about 50 MW of fusion power was needed for GCFTR-2 to sustain a fission power of 3000 MW with a multiplication factor of 0.95^{3,4}. This indicates that a fission power of 3000 MW can be maintained as low as $k_{\text{min}} \approx 0.8$ by a fusion neutron source rate corresponding to $P_{\text{fus}} \propto 200 \text{ MW}$. As shown in section VI, it may be possible to increase the fusion neutron source power to about 500 MW by increasing the current by ~20% if the physics database is extrapolated somewhat beyond the present limits, which would result in an even lower tolerable $k_{\text{min}} \approx 0.5$ for operation at 3000 MW fission power. It should be noted that k_{min} is the subcritical neutron multiplication factor, which is different than the eigenvalue k_{eff} , but using $k_{\text{min}} \approx k_{\text{eff}}$ provides useful guidance.

In order to gain some insight into the effect of fuel depletion on the range of the multiplication constant, a series of calculations was made for the pure TRU fuel. In these calculations, the fuel was uniform throughout the core, was not shuffled, and was uniformly depleted at 3000 MWth, over 600 day intervals, using ORIGEN¹⁶. The multiplication constant was calculated for the fresh fuel and after each 600 day depletion interval, yielding a depletion reactivity decrement $\Delta k/k \approx -0.25$ at 3000 days uniform depletion. As discussed in section VII, the fuel will be burned five times, in different annular locations, so that in the steady-state fuel cycle the core will contain in any burn cycle fresh fuel, fuel that is once burned, fuel that is twice burned, fuel that is thrice burned and fuel that is four times burned.

2. Effect of Heating and Current Drive Ports on Multiplication Constant

One major change in the GCFTR-3 core from the original GCFTR design^{3,4} is that 20 degree sectors have been removed from opposing sides of the annular reactor to make

room for access ports for the bringing heating and current drive (H&CD) power into the plasma, as shown in Fig. 8. These sectors are 20 degree (in the toroidal direction) wedges with respect to the central vertical axis removed from the annular reactor core, shield, and the first wall outboard of the plasma region.

Calculations of the annular core with no sectors removed and with two 20 degree sectors removed were made using the EVENT 'x-y' model to determine the effect of H&CD sector size on k_{eff} . The change in k_{eff} from a fully annular core to one with 20 degree sectors removed 180 degrees apart was approximately one percent, which established that removal of 20 degree sectors do not have a large reactivity effect.

C. Tritium Breeding Blanket

A Tritium Breeding Blanket containing Lithium-Oxide is shown in Fig. 8, and 9. This blanket surrounds the core and the plasma fusion source to breed tritium in order to fuel the plasma. To maximize the amount of tritium produced, a series of calculations was performed using ORIGEN in addition to iterative calculations to determine the optimal configuration of different Li-6 and Li-7 concentrations. The resulting composition of the Li_2O blanket varies in enrichment from 30% to 90% Li-6. This configuration is shown in Fig. 10.

The power of the fusion source will vary from ~50 MW up to at most 500 MW. It is assumed that the variation in source rate will be linear to compensate the linear drop in k_{eff} . The Tritium Breeding Ratio ($\text{TBR} = \text{T produced} / \text{T consumed}$), which is the time-averaged value of the ratio of the tritium produced in the lithium blanket divided by the tritium consumed in the plasma, is a conventional measure of the capability for tritium self-sufficiency.

Tritium is removed from the Li_2O by a helium purging system, then processed to separate it from the helium and other impurities present and stored to await injection into the plasma. It is assumed that the GCFTR will operate in burn cycles of 600 days with a shutdown of 2 weeks between cycles for fuel shuffling. There must be enough excess tritium at the end of a cycle to allow for a two week decay and then to provide for at least a week of fusion operations in the next cycle until the online tritium gas purging and tritium processing system can begin providing fresh tritium. We estimate that $\text{TBR} = 1.1$ is needed to produce adequate tritium for self-sufficiency, allowing for decay, tritium

loss, and purging loss. Using the EVENT x-y model, the neutron flux in each of the lithium regions was determined. Knowing the volume of each region and the incident flux, tritium production was simulated in ORIGEN-S for short intervals (1 day) as to minimize the effects of tritium decay. For the GCFTR, a TBR of 1.08 was determined.

Tritium accumulation calculations were performed in order to determine whether the amount of tritium produced during operation is enough for the plasma to be self-sufficient. The total mass of the lithium blanket is $2.24\text{E}+5$ kg, and the total volume of the lithium blanket is $7.07\text{E}+7$ cm³. Calculations used the flux distributions from the EVENT r-z model in ORIGEN-S to irradiate and decay the lithium in the blanket.

The amount of tritium that must be produced over a burn cycle for self-sufficiency is the amount required to replace the tritium burned over that burn cycle and to provide for one week of operation after restart, allowing for a 60-day decay between shutdown and restart of the next cycle. For the 600 day burn cycle, this requirement is for the production of 63.8 kg over the cycle. The calculations described above predict the production of 64.1 kg over the cycle, from which it may be concluded that the GCFTR-3 is tritium self-sufficient.

Lithium oxide (Li₂O) was chosen as the form for the blankets due to its high atomic density compared to other forms of lithium (Li₂TiO₃, Li₂ZrO₃, etc.). On-line extraction of tritium from Li₂O requires operation between 400 °C and 800 °C. Below 400 °C the rate of tritium diffusion out of the individual grains of Li₂O is too slow, and above 800 °C the particles swell and seal off porous channels through which the tritium must percolate to reach the helium purging channels.

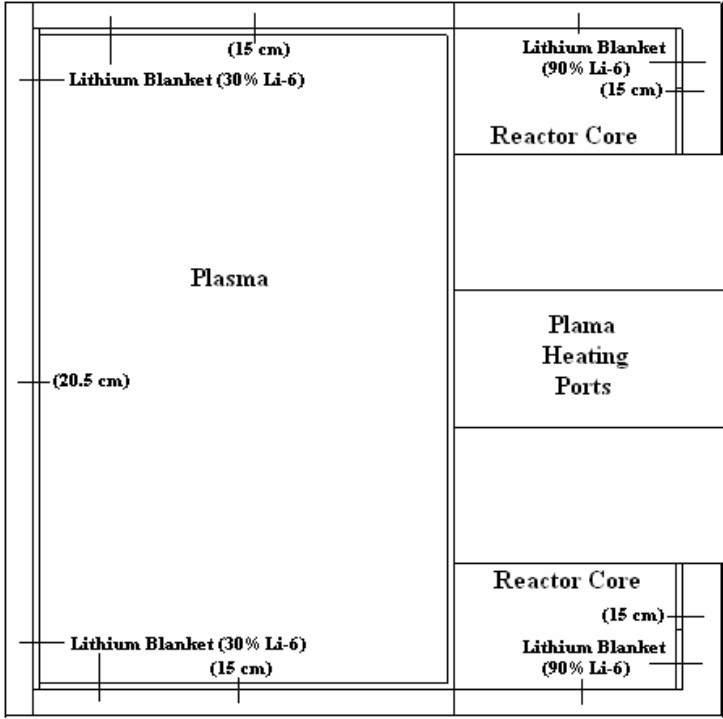


Figure 10: Lithium-Oxide Blanket Location and Enrichment

D. Power distribution

The power distribution of the fission core was calculated with the EVENT x-y model. The total integrated power over the annular reactor core is approximately 3000MW_{th}. This includes only the power generated in the fission core.

Figure 11 shows the normalized radial flux profile over the five core regions for a uniform core at the beginning and end of a 600 day cycle. The distribution is almost symmetric at beginning of cycle when the fusion neutron source (located at left boundary) is small, but the effect of the increased neutron source at the end of cycle is apparent.

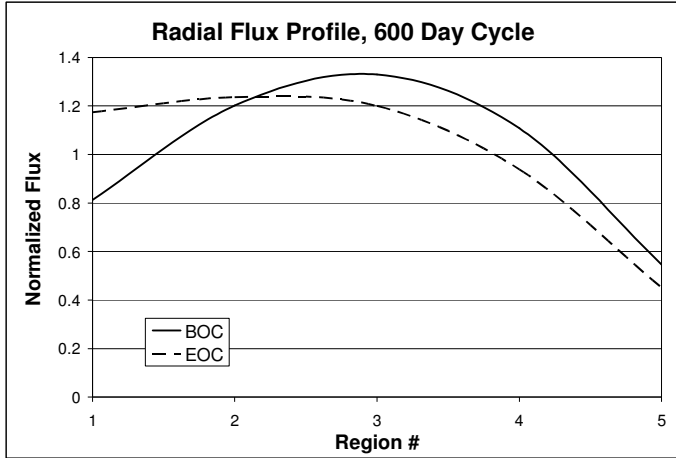


Figure 11: Radial Flux Profile over Five Core Regions

E. Neutron Energy Spectrum

Figure 12 displays the neutron energy distribution in the five regions of the fission core and in the tritium breeding blanket surrounding the core. The neutrons in and surrounding the fission core are fast with essentially no thermal energies present. The neutrons leaving the fusion source are approximately 14 MeV, however they are moderated by the material surrounding the plasma chamber. The spectrum in the first core region next to the neutron source is similar to that for regions further away from the source--a broad spectrum with a mean energy of approximately 1 MeV--except for a small 14 MeV tail. In the tritium breeding blanket there is a prominent dip in the energy distribution slightly below 1 MeV due to resonance absorption due to Lithium-7.

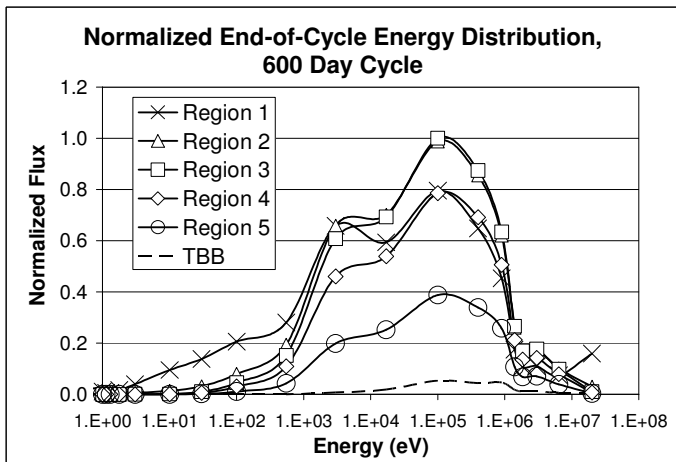


Figure 12: Neutron Spectra in Fission Core Regions and Lithium Blanket

F. Safety

1. Doppler Temperature Coefficient of Reactivity

Doppler feedback is important for the inherently safe operation of the GCFTR-3. Calculations made using KENO found that the core had a temperature coefficient of -0.9065 ± 0.112 pcm/K for pure TRU fuel. A reduction of one standard deviation in the temperature coefficient would yield a value of -0.7945 pcm/K, which would be considered the most conservative KENO estimate. This calculation was repeated with the EVENT r-z model and produced -0.5885 pcm/K.

The Doppler coefficient increased to -1.2775 pcm/K with the addition of 40% U-238 in the fuel, as shown in Fig. 13. These calculations were made using KENO by varying the temperature in incremental steps from 800 °C to 1100 °C for each fuel material composition in the core.

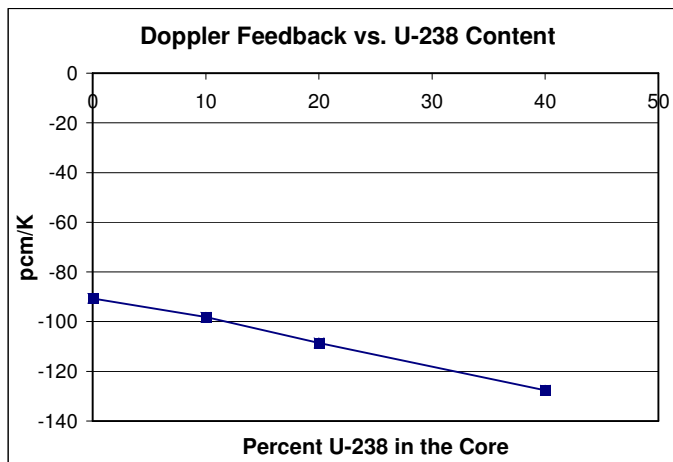


Figure 13: Doppler Feedback vs. ^{238}U Content

2. Reactivity Worth of Core Voiding

In the event of a complete Loss of Coolant Accident (LOCA), the entire inventory of the helium coolant would be voided from the core. (A detailed analysis of the LOCA is provided in Section V.) To quantify the reactivity insertion due to a complete helium blow down, calculations were made using the EVENT x-y model. The results of this calculation showed a positive reactivity insertion of 119 pcm for complete loss of He from the core.

3. Lithium Injection Module

Another aspect of inherent safety that was studied is the use of Li-6 as a shutdown mechanism. Calculations were performed to obtain the amount of lithium that would be required to add approximately five dollars of negative reactivity into the core. The EVENT x-y model was used with various amounts of Li-6 and Li-7, which were added to quantify their effects and compare the two isotopes. Using Li-6 produced far better results than Li-7. A comparison of the cross sections of Li-6 and -7 showed that the absorption in the fast energies was approximately the same. The model determined that $5E+19$ atoms/cc of Li-6 would be required to introduce five dollars of negative reactivity. Considering the total volume of the reactor, this is approximately 600 grams of lithium enriched to 95% Li-6.

Considering the concept of a Lithium Injection Module³⁹ (LIM), after the temperature reaches a certain threshold the lithium is released into the core. The LIM consists of a chamber located directly above the core in which the lithium is stored beyond a seal. The chamber is pressurized with gas that effectively pushes the lithium into the core after the seals have been broken.

G. Shield

The primary purpose of the shield is to protect the superconducting toroidal field coil magnets from radiation damage. The shield also reduces radiation levels to an acceptable rate for other components. The maximum allowable dose rate^{3,4} limit to the superconducting magnet insulators over a forty year period at 75% availability is 10^9 - 10^{10} rads, depending on the insulator, the lower of which equates to 7.922 rads/sec. The maximum allowable^{3,4} fast neutron (>0.1 MeV) fluence to the superconductor is 10^{19} n/cm². The shield was modeled using MCNP with a volumetric neutron source representing the fusion plasma. The fusion neutron source energy had a Gaussian distribution around 14 MeV. Calculation of the flux was based on an average surface tally flux approximation. A surface tally counts the number of neutrons that hit a defined surface, giving a total tally of the flux (or neutrons per cm² per second) over that surface. To simplify the core, the fuel was modeled as a homogeneous mixture throughout each of the five equal-volume annular core regions.

The decision to remove two 20 ° sectors from the reactor and surrounding shield imposed a demanding constraint on the design of the shield. Extra shielding is required to reduce leakage from these H&CD ports. Shielding around the sectors was composed of the same materials and thicknesses as the main shield.

Four annular regions of different shielding materials were used for the GCFTR-3 design. The specific composition and density of each layer is given in Table 7. This shield surrounds the lithium-oxide blanket region.

Table 7: Shield Layers and Compositions

Layer	Material	Thickness	Density
Reflector	ODS Steel	3.5 cm	7.9 g/cc
1	Iridium (Ir)	4.75 cm	22.4 g/cc
COOL A	Helium (He)	0.25 cm	0.1785 g/cc
2	Cadmium (Cd)	0.95 cm	8.65 g/cc
COOL B	Helium (He)	0.05 cm	0.1785 g/cc
3	Boron-Carbide (B ₄ C)	4.5 cm	2.5 g/cc
4	Tungsten-Carbide (WC)	4.5 cm	15.7 g/cc
COOL C	Helium (He)	1.0 cm	0.1785 g/cc
5	Hafnium-Carbide (HfC)	38.25 cm	12.76 g/cc
6	Tungsten-Carbide (WC)	4.5 cm	15.7 g/cc
COOL D	Helium (He)	2.25 cm	0.1785 g/cc

Iridium, hafnium carbide, tungsten carbide, and boron carbide were chosen as shielding materials to thermalize and then absorb fast neutrons and gammas, while the cadmium layer was selected primarily to absorb neutrons. In addition, the entire shield was modeled to operate between 400-800 °C.

Allowing for a maximum operating power level of 500 MW for the fusion neutron source, it is calculated, from MCNP, that the magnets will remain functional for their anticipated lifetime of 40 years at 75% availability and that the nuclear heating of the magnets will be modest, as indicated in Table 8. The main shielding layer, B₄C, will show a substantial depletion at this point resulting in an increase of the neutron flux at the magnets.

Table 8: Shielding Performance

Parameter	Limiting Dose ^a	MCNP Result	Time to end of life
40-yr Fast Neutron Fluence to Superconducting Magnets at 75% availability	10^{19} n/cm ²	1.57×10^{18} n/cm ²	> 40 years
40-yr Radiation Dose to Magnet Insulators at 75% availability	10^9 - 10^{10} rads ^b	3.06×10^7 rad	> 40 years
Nuclear Heating in the Magnets		34.5 kW	
Power for cooling toroidal magnets		3.9 MW	

^aRef. 3 and 4; ^b epoxy/ceramic

Helium coolant channels were sandwiched between each of the four layers of the shielding materials. The use of xenon coolant instead of helium coolant to enhance the absorption of thermal neutrons was considered. A comparative analysis determined that despite the significantly larger thermal cross section of xenon, there was only negligible difference in the performance of the shield because of the small number of thermal neutrons. After considering the heat removal capabilities of the two coolants, helium was chosen as the preferred coolant.

V. THERMAL

A. Core Thermal Analysis

The fuel pin design was modeled after a standard PWR pin, which consists of three layers. The inner material is composed of TRISO particles bound by a silicon carbide matrix into a cylindrical pin 0.6 cm in radius, as was described in section III. A 0.01 cm helium gas-filled gap comprises the second layer of the fuel pin to account for thermal expansion. The final layer consists of a 0.06 cm oxygen dispersion strengthened (ODS) martensitic steel (which is represented by the thermal properties of HT-9 steel) cladding.

The reactor operates at a distributed power of 3000 MWt, with an average volumetric heat generation rate of $q''' = 42.2$ MW/m³. The thermal analysis performed on the fuel pin followed the form of a thermal circuit⁴⁰. Values used in the circuit are presented in Table 9.

Table 9: Fuel Pin Thermal Conductivities.

Pin Component	Thermal Conductivity (W/m-°C)
---------------	-------------------------------

Silicon Carbide	120
TRISO kernel	27.6
Zirconium Carbide	18.94
Tungsten Carbide	84.02
TRISO particle (Homogenized)	47.8
Fuel Pellet (Homogenized)	55.14
HT-9 Steel	29
Helium Gap	0.26

The value for the fuel pellet thermal conductivity was obtained by homogenizing the TRISO particle thermal conductivity with the silicon carbide matrix thermal conductivity based upon the mass percents of the materials. The gap coefficient was obtained from a previous study³. Using 33% of the melting point of the HT-9 steel cladding, 445°C, as a limiting factor, the heat transfer coefficient for the helium coolant was found via the thermal circuit to be 4323 W/m²-°C.

Applying the thermal circuit method, a distribution of bulk temperatures was calculated. The results are presented in Fig. 14. The lowest melting point of the materials comprising the fuel pin is the clad, which is 1327 °C. Any effect of neutron irradiation on the thermal conductivity has not been taken into account.

The mass flow rate of the helium coolant was found to be 3280 kg/s, which corresponds to a velocity of 94 m/s. A pumping power of 0.172 MW is required to pump the helium at a rate fast enough to keep the clad temperature at 33% of the melting temperature.

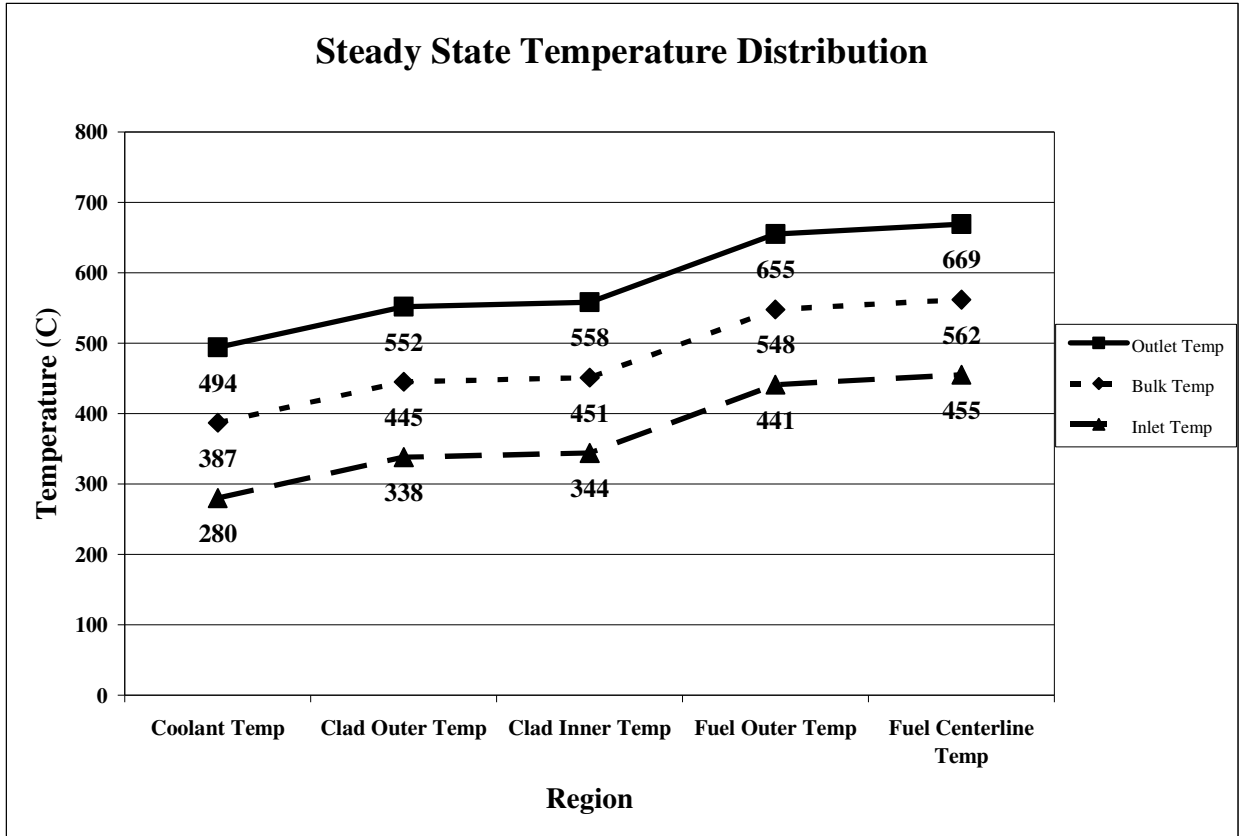


Figure 14: Fuel Pin Temperature Distribution

B. Secondary Power Conversion System

The GCFTR-3 is a power-generating reactor. With helium as the coolant for the channels within the core, it is possible to use a direct Brayton Cycle and bypass a heat exchanger, as indicated in Fig. 15. A secondary system for heat transfer and electric power generation must be established to operate the flow of the hot and cold legs attached to the cooling channels. For power generation analysis, the thermodynamic properties of the coolant fluid were evaluated. The system's legs were assumed to be in physical connection to the physical upper (hot) and lower (cold) extremities of the cooling channel itself. The piping mechanism is flexible but a singular secondary is modeled for this design.

Although thermal-to-electric efficiency would be of concern to a utility, the main focus of the GCFTR-3 is deep burn of the transuranic fuel, and avoidance of problems associated with high-temperature materials was favored over potential high thermal efficiency. With the assumption of 3 GWth produced in the fission core, certain thermal parameters were calculated. Helium gas is known to have a specific heat capacity of 5193 J/kg-K. The temperature in the hot

leg was chosen as 300°C. Past the compressor the fluid is 494°C at 7 MPa. After leaving the turbine, the temperature is 122°C and the pressure is 2.4 MPa. After the cooler, a state of 151°C and 7 MPa is fed back into the cold leg. These values, in consideration of thermal input and electrical output, factoring in operation power requirements, amount to an efficiency of 34 %. This results in an actual power generation of 1020 MWe.

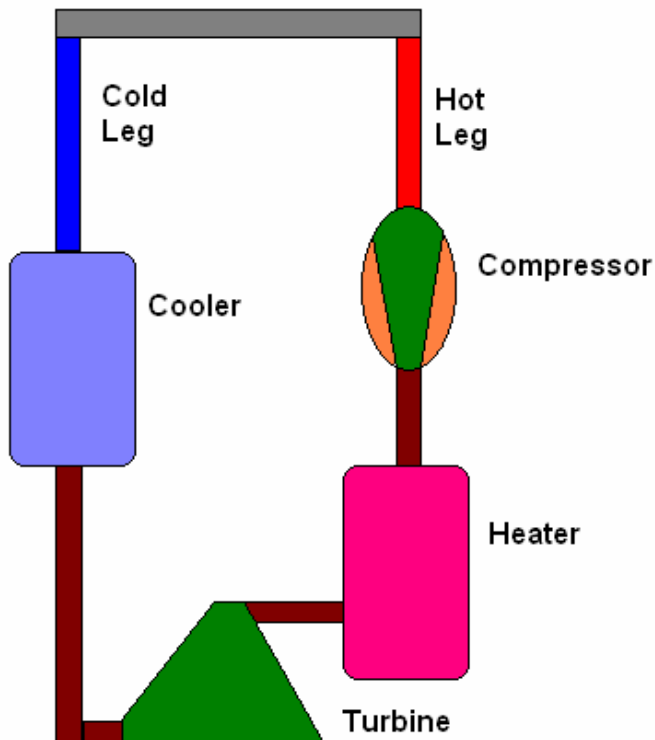


Figure 15: Direct Brayton Cycle

C. Loss of Coolant Accident (LOCA)

In order to determine the appropriate response for a large scale coolant accident, a thermal analysis of the core was performed under the conditions that would exist during a severe LOCA. A design basis complete loss of coolant accident was postulated. The break was assumed to be sufficiently large so that any helium in the core immediately escaped into the containment building, resulting in a rapid pressure drop (to 0 psig) and complete loss of normal core cooling. It was assumed that the neutron source was immediately shut down and that all heat addition came from decay heat calculated using the ORIGEN-¹⁶ code. Figure 16 displays the decay heat for two different fuel compositions. C1 represents previous work on the GCFTR-2 with 100% TRU fuel being burned for 1825 days³. C2 represents the current work with an

increased burnup of 3000 days and a new mixed fuel composition of 70% TRU/ 30% U-238. The large increase in decay heat can be attributed to the increase in burn time which provides for more fission products and actinides.

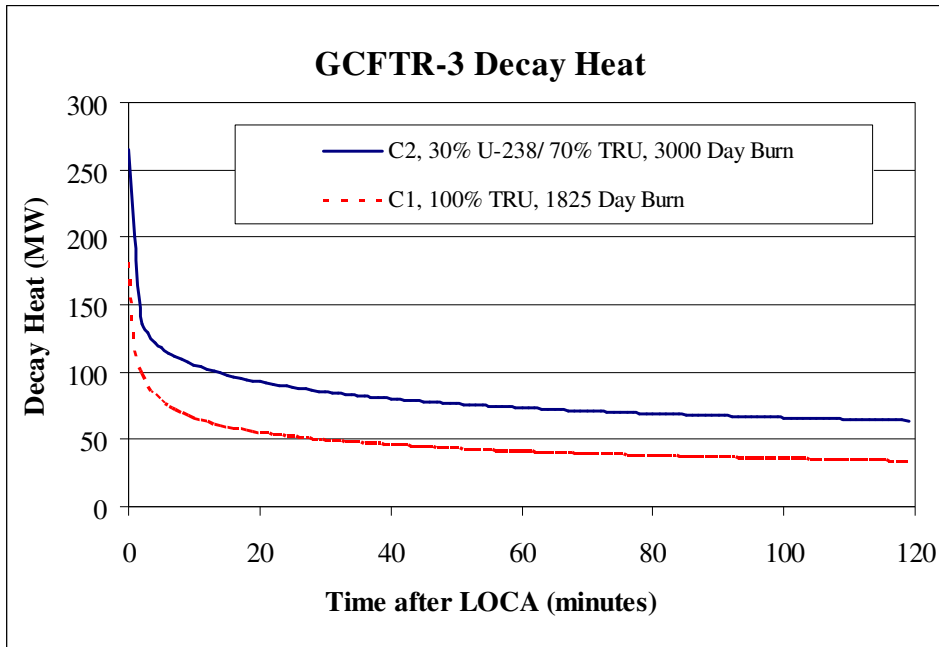


Figure 16: Decay Heat

Once the coolant is lost, the only significant process for removing heat from the core is thermal radiation transfer. Because sophisticated computer modeling would be needed to simulate this process for the entire core, a comparison was made between the GCFTR-3 and the annular core of a helium cooled Prismatic Fueled Reactor (PFR) in which a detailed calculation of the amount of heat rejected from the core as a function of time had been made⁴¹. Although the PFR design differed in heat capacity, the general analysis was formulated as a hot surface radiating heat in which the time-dependent temperature of the PRF following a LOCA was already known, thus providing a means to estimate the capability of the core to radiate heat.

In order to adjust the PRF values for the GCFTR-3, a scaling factor based on geometry and the Stefan-Boltzmann Law was derived. The parameter included a multiplication constant of 2.2 which was taken as the product of a ratio of surface areas of the GCFTR-3 and PFR with a temperature ratio raised to the fourth power to compensate for the dependence of radiation transfer on temperature. The modified rejection heat was then subtracted from the GCFTR-3 decay heat to provide a value for the overall heat stored in the reactor core as a function of time.

To determine the temperature rise caused by the lack of coolant, the temperature change was related to the mass, specific heat and stored heat of the reactor core. The average specific heat of the core was approximated by averaging the different materials within the core and weighting them by total mass. The overall mass of the core was calculated from known fuel masses with a 15% increase for structural material not included in the fuel values. Using these parameters along with the stored heat values, the temperature change was calculated at intervals of one minute during the first hour after the LOCA, with the scaling factor for rejection heat being updated iteratively to account for the increase in temperature. Figure 17 displays the temperature rise along with the melting temperature for two different clad materials. Without emergency core cooling it was determined that the core would experience significant damage two minutes after a complete loss of coolant. The clad temp peaks soon after at 2465°C, at which point the core begins to radiate more heat than is accumulated from decay due to the dependency of radiative heat transfer on temperature.

In comparison with previous work³ which calculated clad temp during a LOCA by direct computer simulation, the current method for assessing a LOCA produces roughly similar time scales and temperatures. The overall melt times and maximum temperatures however, cannot be accurately compared due to different burnup conditions used in the previous analysis. What can be concluded is that it becomes progressively harder to survive a LOCA as burn time is increased. In the shift from an 1825 to 3000 day burnup, the added decay heat increases the clad temperature at every point by approximately 300°C.

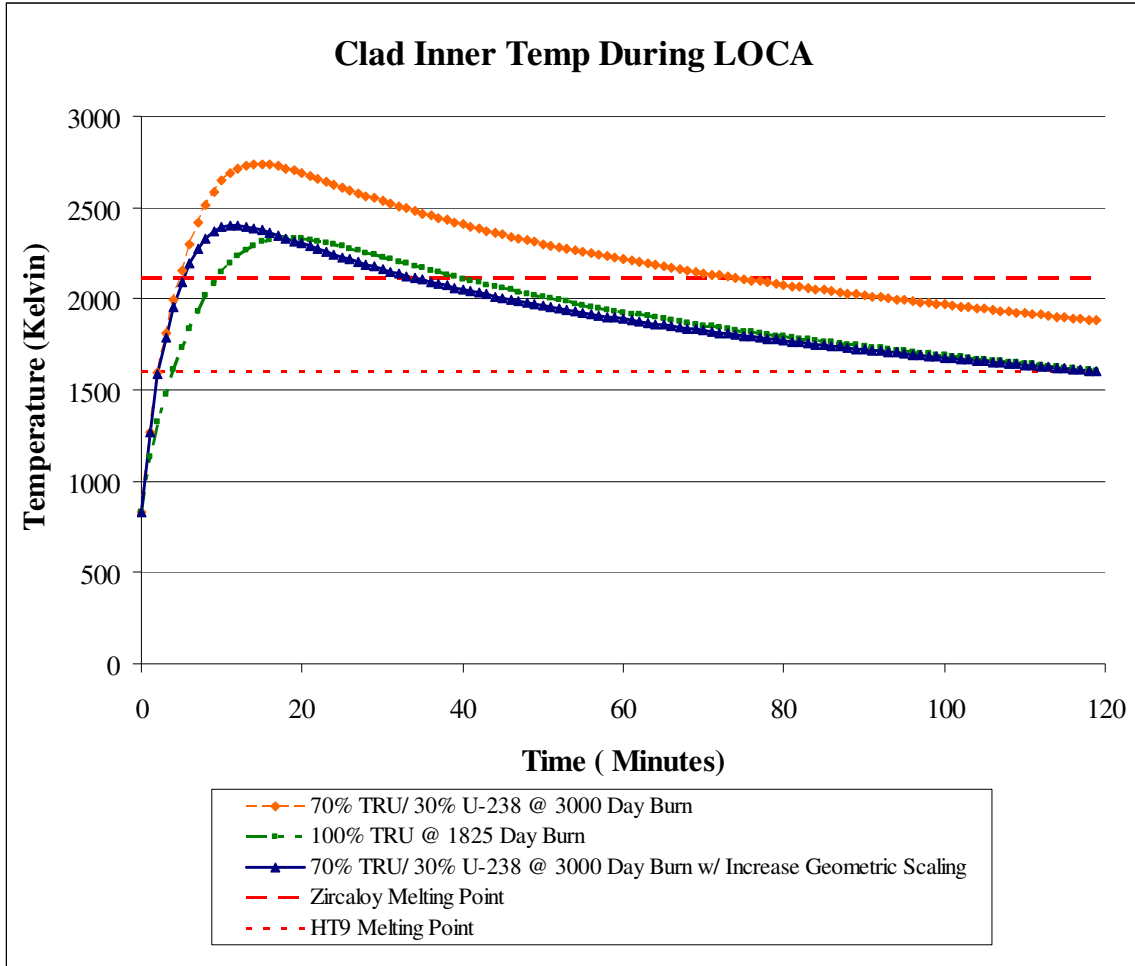


Figure 17: Clad Temperature during LOCA

With the higher burnup it becomes extremely difficult to lower the core temperatures to a safe level. Even with the addition of large heat sinks which raise the average thermal capacity of the core, the time to melt still retains a value below 10 minutes. In order to reduce the maximum temperature or decrease the amount of time needed from an emergency core cooling system, the only parameter capable of significantly altering the temperature rise is the geometric scaling factor. By increasing the ratio of surface area from 2.2 to 4 as shown in Figure 17, the maximum temperature decreases 330°C and the time needed from an ECCS is greatly reduced. These results suggest that an increase in the total surface area, either through the use of fins or an increase in volume, would help mitigate some of the damage inflicted by extreme temperatures and help reduce the load on an emergency core cooling system.

D. Emergency Core Cooling System (ECCS)

Both the above LOCA analysis and a previous analysis³ of the same core demonstrate that while long term core cooling via only natural means (i.e. radiation and convection) is viable, the decay heat load immediately following a LOCA is high enough to initiate cladding failure in under 10 minutes. Consequently, a means of short term emergency core cooling is necessary to ensure safe cladding temperatures under all conditions.

Consistent with passive safety design goals, an accumulator system was designed to provide emergency core cooling. The accumulator was engineered to meet several critical design criteria: passive actuation and injection, adequate coolant injection rates under all credible core conditions (i.e. decay heat loads) and sufficient injection time to allow decay heat loads to reduce to safe levels.

The final accumulator design was a ring header in the shape of a torus, which can be located either above or below the reactor. Attached to the torus are twenty-four 55m³ standby helium tanks. The torus is connected to the reactor via four 6" ID injection headers, each containing a flow restrictor and check valve in series and the entire system is pressurized to 6.5MPa. The accumulator system uses no components that require operator action or power and thus is considered a passive safety system. It uses no pumps, compressors, control circuitry, or power operated valves. Under normal conditions, reactor pressure seats the check valves in the injection headers thereby isolating the accumulator from the reactor.

Upon initiation of a LOCA, reactor pressure decreases rapidly. This drop in reactor pressure causes a difference between accumulator pressure and reactor pressure, thereby driving the helium in the accumulator into the reactor vessel via the natural pressure differential. Early in the accident sequence (when decay heat is high) the differential pressure between the accumulator and the reactor is also high, resulting in a high flow rate and heat removal rate (see Table 10). As the accumulator's helium supply is diminished, the driving pressure is also reduced and the injection rate will drop accordingly. The use of flow restrictors in the injection lines is critical to ensure that the helium supply does not deplete too quickly and that injection rates are appropriate for their corresponding decay heat loads.

The size of the accumulator, minimum coolant mass, flow restrictor properties, and standby pressure are primarily functions of the worst case decay heat load and core flow parameters. First, a limiting clad temperature was selected; this value was determined to be 1500 K, approximately 100 K below the ODS clad melt temperature. Next, a convection coefficient, h was calculated that would provide sufficient cooling so as to maintain this cladding temperature

under the decay heat load at any given time. Based on this convection coefficient, a Nusselt number and Reynolds number for coolant injection were determined⁴². From the Reynolds number, a coolant velocity and mass flow rate were determined. The mass flow rate was used to determine a minimum adequate driving pressure and flow restrictor coefficient⁴². Each of these values was calculated at various points in time during the first 2 hours of the LOCA. The mass flow rates were integrated to determine the necessary standby coolant mass and the accumulator volume was selected to meet driving pressure requirements.

Various safety factors were applied to ensure appropriate margin (with respect to maximum cladding temperature) and to account for any design uncertainties. The decay heat loads were conservatively selected by modeling a burnup of 3000 days for the entire core, rather than just one fuel batch. This led to a substantial rise in decay heat over previous analyses³ and provided a conservative bounding heat load for ECCS. Calculated convection coefficients were divided by a factor of 2 to account for any unforeseen reductions in coolant flow during the accident and to account for peaking factors. Finally, although LOCA analyses have shown that peak cladding temperatures approach (but do not exceed) the melting point, this condition exists for only a brief period of time. See Table 11.

Figure 18 demonstrates the effectiveness of the accumulator. Note that margin is maintained between peak cladding temperature (1500 K) and clad melt temperature (1600 K). Also of interest is that the accumulator system substantially suppresses cladding temperatures throughout the duration of the transient, thereby maintaining temperatures at safe values well beyond the point where peak cladding temperature is reached.

Table 10: ECCS Injection Velocities and Coolant Flow Rates

Time after LOCA (min)	Coolant Velocity (m/s)	Coolant Flow Rate (m³/s)
1	17.33	66.00
5	16.81	63.95
10	16.30	62.10
15	16.03	61.08
30	14.49	55.13
45	12.93	49.19
60	11.63	44.27
90	8.14	30.95
120	0.25	27.46

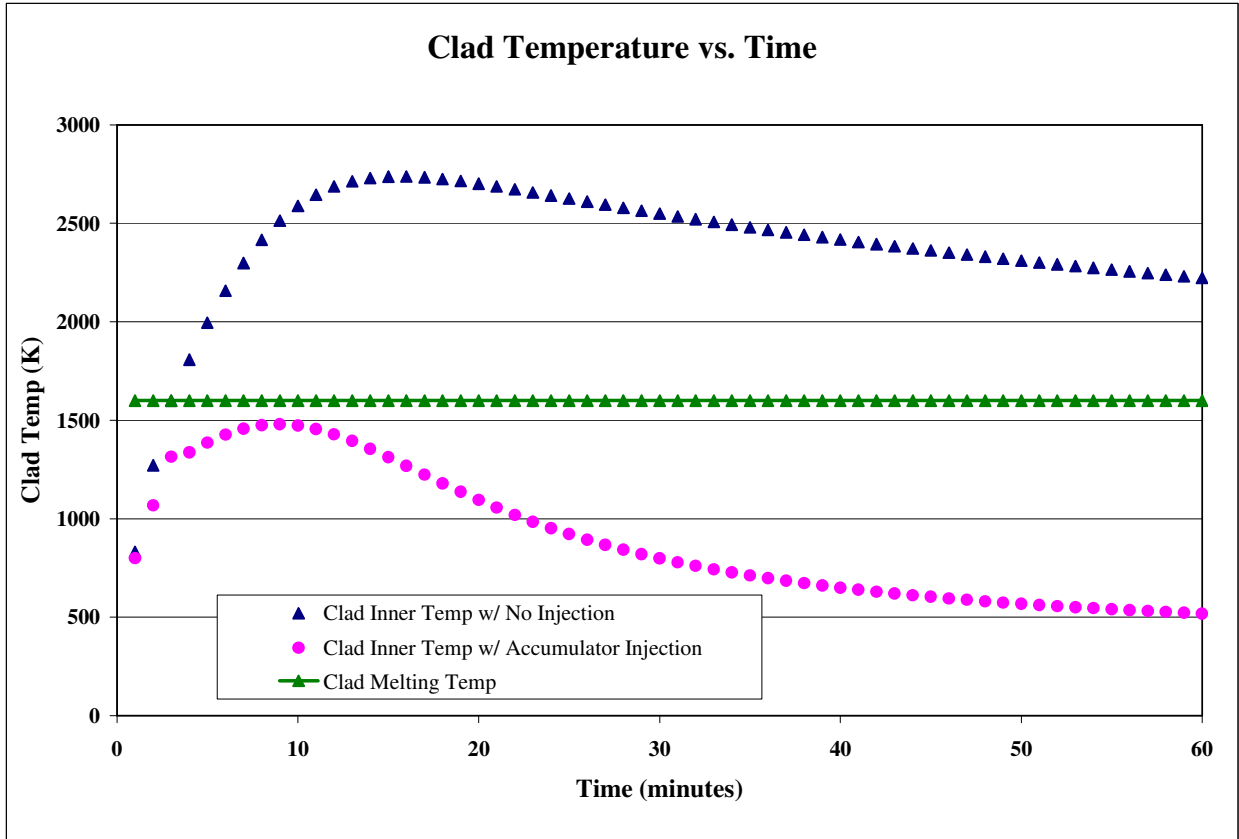


Figure 18: ECCS effect on cladding temperatures

Table 11: Clad Temperature Safety Margins

Time after LOCA, minutes	Cladding temperature, K	Margin ($T_{\text{clad}} - T_{\text{melt}}$), K
5	1386.8	214.2
9	1479.9	120.1
15	1312.4	287.6
25	921.5	678.5
35	711.7	888.3
60	518.0	1082.0

VI. FUSION NEUTRON SOURCE

A. Neutron Source Strength Capability

A neutron source design task for GCFTR-3 was to determine the maximum neutron source strength possible without changing the dimensions of the GCFTR-2 neutron source in order to allow operation at the lower values of k_{eff} associated with higher fuel burnup. To this end, increases of normalized beta, H-factor, and current that can provide for an increase of fusion power up to about 500 MW were investigated. A fusion performance code, called IACODE, was used for systems analysis of plasma performance. The code is based on the equations in Ref. 43 and detailed in Appendix D. The plasma parameters in Table 12 were inputs and thereby represent physical constraints.

The target operating fusion power was 500 MW, which is large enough to sustain the 3000 MWth power in the fission reactor down to $k_{\text{eff}} \approx 0.5$ (see section IV). The design of the tokamak fusion neutron source for the previous GCFTR-2 design³ was based on normalized $\beta_N \leq 2.5$, H-mode confinement enhancement factor $H^{ITER98} \approx 1.0$ and plasma current $I = 8.2$ MA. The effects of modest increases of these parameters on fusion power were evaluated, subject to the physics and engineering constraints⁴³ described in Appendix D.

Table12 Constrained Parameters for Performance Evaluation.

Constrained Parameter	Value
Toroidal (Major) Radius	3.75 m
Plasma (Minor) Radius	1.08 m
Magnetic Field of TF coil	11.8 T
Plasma Elongation	1.7
Plasma Triangularity	0.4
% Greenwald Density Limit	75
Allowable Field Swing in CS	26.3 T

Figures 19 and 20 show how β_N and the H-factor affect the total power and the required auxiliary power at currents of 9 MA and 10 MA, respectively, using the constraints listed in Table 13 and in Appendix D. Figure 19 shows that with a current of 9 MA, the maximum fusion power is around 400 MW, keeping within acceptable normalized beta and H-factor limits. Figure 20 shows that by increasing the current to 10 MA, a fusion neutron source power of 500 MW becomes possible. Table 13 shows the plasma performance parameters calculated for these two cases using a normalized beta of 0.285. Operating at lower currents requires increasing the H-factor in order to avoid the auxiliary power (design) limit of 100 MW. Table 13 shows that in order to meet this constraint the H-factor must be increased to 1.13 to operate at maximum power, which is an aggressive value and may not be possible. As a result, a current of 10 MA is probably necessary to meet the design objective of 500 MW fusion power without exceeding 100 MW of auxiliary power.

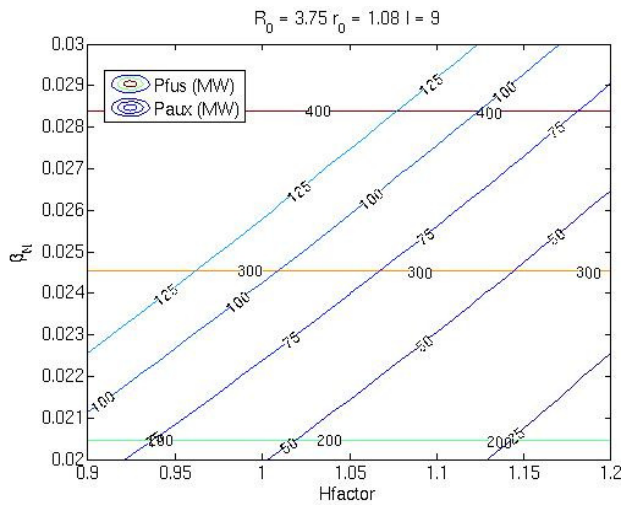


Figure 19: Fusion Power at I=9 MA.

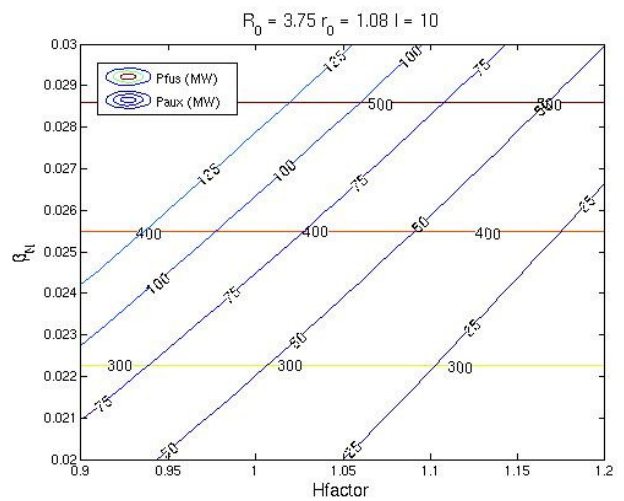


Figure 20: Fusion Power at I=10 MA.

Table13: Performance characteristics for 9 MA and 10 MA fusion neutron sources.

Plasma Parameter	I_p = 9 MA	I_p = 10 MA	ITER I_p=15 MA
Total Fusion Power (MW)	403	498	410
Neutron Source (10 ¹⁹ /s)	14.2	17.5	14.4
Auxiliary Power (MW)	98.6	98.2	
Plasma Power Amplification, Q _p	4.1	5.1	10.0
Normalized Beta, β _N (%)	2.85	2.85	1.8
Toroidal Beta (%)	4.036	4.485	
H-factor	1.13	1.06	1.00
Energy Confinement Time (sec)	0.726	0.737	
L-to-H Threshold Power (MW)	27.1	28.73	
Safety Factor, q ₉₅	5.472	4.01	
Volt-Seconds for Startup	98.5	107.3	
Bootstrap Current (MA)	2.63	2.55	
CD Efficiency (10 ⁻²⁰ A/Wm ²)	0.456	0.58	
Electron Density	1.84x10 ²⁰	2.05x10 ²⁰	
Toroidal Magnetic Field (T)	5.9	5.9	
Poloidal Magnetic Field (T)	1.2	1.3	
Neutron Wall Flux (MW/m ²)	1.45	1.78	0.5
FW Heat Flux (MW/m ²)	0.32	0.35	0.15

B. Adaptation of ITER Divertor to Helium Coolant

1. Overview of Divertor

The heat exiting the plasma across the last confined flux surface is swept along field lines into the divertor chamber and deposited over a relatively small area on the divertor target. This produces a very high heat flux on the divertor, of order 5 MW/m² for ITER and 1-2 MW/m² for GCFTR-3, during normal operation, with much higher peaks during disruptions. To handle this heat flux, the ITER divertor employs either carbon fiber, carbon, or tungsten tiles, joined to copper blocks. The copper blocks are hollow with a smooth tube or a swirl tape along the tube, allowing coolant to flow, and are assembled on the inner and outer vertical targets, as well as the divertor dome. For each of the 54 divertor cassettes, coolant flows in series first through the outer vertical target, then the inner vertical target, and then through the dome. Fig. 21 shows a picture of a divertor cassette with a cross section of the copper block assemblies, and Fig. 22 shows the coolant flow through each cassette.

Water is the coolant for ITER, but because helium is the primary coolant for GCFTR-3, a thermal analysis to determine whether helium can cool the divertor was made. Adapting the coolant from water to helium has the main advantage of simplifying the plumbing for GCFTR-3 and avoids having different coolants for the fission and fusion components. In order to facilitate the adaptation to helium, the coolant flow for the GCFTR-3 will not be in series, as is the case for ITER, but will have individual coolant loops for the inner vertical target, outer vertical target, and dome.

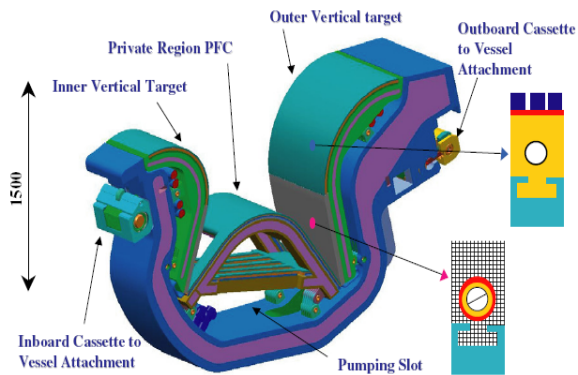


Figure 21: Divertor Cassette⁴⁴

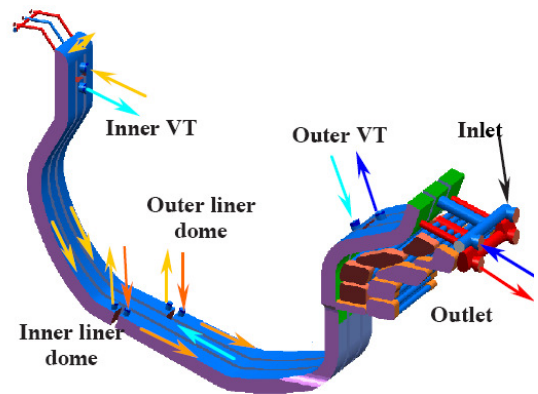


Fig. 22: Divertor coolant flow⁴⁵

2. *Thermal Analysis for Helium Coolant*

Divertor heat removal was modeled analytically, as described in Appendix D, based on straight pipe flow that is a certain distance below a uniform heat flux. Heat removal was also analyzed in three dimensions using Fluent⁴⁶, which solves the energy equation coupled with the Navier-Stokes equations. A three-dimensional model and mesh for one cooling channel of the outer vertical target, created using Gambit⁴⁶, consists of a copper block with a smooth tube. The analytical calculations of the maximum surface temperature of the block and average coolant exit temperature, when cooling with water, agreed with those of ITER⁴⁵, giving confidence in using the model to analyze helium. However, operating conditions for helium differ somewhat from water, in that the operating pressure increases from about 4 MPa to 6.5 MPa, helium inlet temperature is 300 K, and helium mass flow rates vary from 0.4 to 1.2 kg/s.

The maximum surface temperature of the cooper block was a major design constraint in the analysis of the coolant channel. Figure 23 shows the Fluent results of peak surface temperature on the cooper block for the mass flow and heat flux region analyzed. The heat flux was modeled as a uniform heat flux on the entire plasma-facing surface with the initial conditions mentioned previously. Each mass flow rate case was run for seven different heat flux values ranging from 0.5 to 2 MW/m². 773 K was the maximum allowable surface temperature based on literature studies⁴⁷; 696 K and 579 K represent 90% and 75% of the limit, respectively. The Fluent results agreed well with parallel analytical calculations shown in Appendix D. As Fig. 23 shows, using a uniform heat flux approximation results in an achievable heat removal for the 0.5 to 2 MW/m² divertor heat flux range anticipated for normal operation of GCFTR-3.

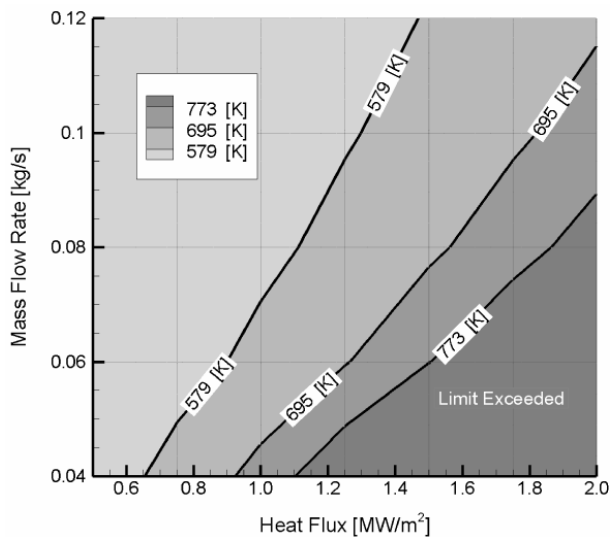


Figure 22: Maximum Surface Temperature.

The mass flow rate range analyzed corresponds to an inlet velocity range of 60 m/s to 190 m/s. This velocity could be reduced by increasing the cross-sectional area of the channel. For this study, the flow tube is 10 mm in diameter, maintaining ITER's dimensions. The Fluent results show that a channel could sustain 1 MW/m² and avoid failure at the 60 m/s inlet velocity range, while an inlet velocity of 143 m/s would be required for 2 MW/m².

Based on the pressure drop across the channel that Fluent converged upon, the pumping power per channel was calculated. This calculation indicates that a 1 MW/m² heat flux at 0.04 kg/s would require approximately 250 W, and a 2 MW/m² heat flux at 0.1 kg/s would require 4.8 kW, per channel. The ratio of the pumping power to the total heat removed per channel (assuming an 85% pumping efficiency) results in 0.5% and 6.1% for the 1 and 2 MW/m² cases, respectively. To estimate the pumping power for GCFTR-3, these values were scaled up based on the total number of channels. This yields a total pumping power of approximately 511 kW and mass flow rate of 89 kg/s for the 1 MW/m² heat flux and 10.6 MW with 222 kg/s for the 2 MW/m² heat flux. This may be somewhat low since the center dome will require a larger pumping power than the outer targets.

Using results from both the analytical calculations and the Fluent model of the outer vertical target, approximate values were found for the effect of heat transfer enhancement by swirl tape. The enhancement multiplication factors used were 2 for the friction factor and 4 for the convective heat transfer coefficient⁴⁷. These factors only represent a rough approximation of the effect, due to the limited capability of the analytical solution and their uniform application. The solution procedure involved iteration on the friction factor using the Colebrook formula and the Petukhov correlation for Nusselt number^{48,49}. This created a reduction in the required mass flow rate by approximately 45%, and thus a reduction in the pumping power needed to handle the required heat flux loads.

The center dome region of the divertor is approximately 0.8 meters longer than the outer vertical target and thus presents a more limiting case. The analytical model indicates that an approximately 25% increase in mass flow rate would be required to sustain the same heat flux relative to the outer vertical target. The use of swirl tape or other heat transfer enhancement methods would improve the operating limits for the center dome.

Based on this analysis, it seems feasible to adapt the ITER divertor design for use in GCFTR-3 using helium as the coolant.

C. Heating and Current Drive Systems

The proposed ITER H&CD systems incorporate all major electromagnetic wave H&CD systems in use today. Selected components of ITER's systems were implemented in GCFTR-3 because of their desirable properties and GCFTR-3's design constraints. A useful review of H&CD systems and terminology is provided in Appendix D. This section focuses on required properties of GCFTR-3's H&CD system and a description of how ITER's H&CD system was adapted for use in GCFTR-3.

1. Current Drive Requirements

An important part of the GCFTR-3 current drive requirement is the bootstrap current. Since GCFTR-3 is to operate in steady state, it is mandatory that non-inductively driven current plus bootstrap current be equal to the total required plasma current of 9 to 10 MA. The required non-inductively driven current is $I_{cd} = (1 - f_{bs})I_p$. With all the auxiliary power available for current drive and allowing the current drive to be described by the current drive figure of merit

$$\gamma_{cd} = \bar{n}_{e20} R_0 (1 - f_{bs}) I_p Q_p \frac{1}{P_{fus}}$$

we can determine a necessary parameter of our H&CD system.

An empirical formula for the bootstrap current fraction (of the plasma current) is given by the expression

$$f_{bs} = (1.32 - 0.235 \left(\frac{q_{95}}{q_0}\right) + 0.0185 \left(\frac{q_{95}}{q_0}\right)^2) \left(\sqrt{\frac{1}{A}} \beta_p\right)^{1.3}.$$

These formulas are used to evaluate the current drive requirements for the 500 MW_{th} GCFTR-3 tokamak.

The required bootstrap current fraction in GCFTR-3 at steady-state, 500 MW_{th} operation is about 0.25. By comparison, a conservative ITER design value is about 0.5. The bootstrap current for the GCFTR-3 is reasonably achievable by today's standards. Bootstrap currents as high as 80 % have been achieved at low performance in JET⁵⁰.

2. GCFTR-3 500 MW_{th} H&CD Requirements

The current goals of the GCFTR-3 design include power levels that require nontrivial H&CD injected power. It was determined that 100 MW of concurrent power delivery was a reasonable design limit, given technology levels, electrical power

availability, and plasma access limits. With the goal of increasing the tokamak fusion power to $500 \text{ MW}_{\text{th}}$, a H&CD system was researched in order to increase H&CD capabilities while meeting the operational requirements and design constraints of the higher-output tokamak.

An important type of H&CD system is Neutral Beam Injection. However, due to the size, geometric requirements, and complexity of this type of system, it was excluded from consideration. Current drive, which is critical to the operation of GCFTR-3, requires the NBI system to be aligned tangential to the plasma axis. This proves very difficult and impractical with an annular fission reactor surrounding the plasma chamber. Therefore, it was decided to focus on systems that simultaneously provide H&CD while geometrically perpendicular to the plasma axis.

The H&CD requirements are determined to support a fusion neutron source operating at the upper limit believed feasible for the present design (Section VI.A). Several aggressive parameter values were used in the pursuit of this goal in the design. A main parameter increased over past designs is the plasma current. This performance increase raises the requirements of the H&CD system. It is this increase that demands the high current drive figure-of-merit LH system over other more well known systems. Also, the heating power input was augmented to a continuous maximum of 100 MW with a peak output of 120 MW, another aggressive value demanding six 20 MW LH H&CD units. A third demand was to fit H&CD systems in between TFC coils and include shielding. A LH H&CD system provided the correct size, power, and the highest achieved current drive efficiency, albeit being inferior in achieved heating.

The required current drive figure-of-merit for the LH H&CD system at $500 \text{ MW}_{\text{th}}$ fusion power, 10 MA of current, and a bootstrap current fraction of 25% is .577. In 2000, current drive figures of merit as high as .45 were achieved with a LH and ICRF dual-resonance H&CD system⁵⁰. Therefore, with near-term technological advances, expecting the H&CD system to be capable of fulfilling GCFTR-3 design requirements is reasonable. Additionally, higher bootstrap current will be achieved in the future, easing the wave current drive requirements.

The actual LH port designs are based on the port plugs used in ITER. Each port has a power of 20 MW. In GCFTR-3, there are two sections of the annular fission reactor

between the magnets removed on opposite sides of the reactor. This design is based on the need for H&CD system access to the plasma. Because of the highly constrained geometric options, the six 20 MW LH port plugs are centered vertically and toroidally in the outer plasma chamber wall in an arrangement like the one in Fig. 24, with three in each removed reactor section. This type of arrangement has not been extensively tested in tokamaks, but is mandatory in order to provide the required amount of H&CD and allow for magnet shielding in GCFTR-3. Based on the ITER designs, it is expected that each LH H&CD port would provide 20 MW of heating and ~ 1.5 MA of current drive⁵⁰. Table 14 shows a comparison for the GCFTR-3 and ITER H&CD systems.

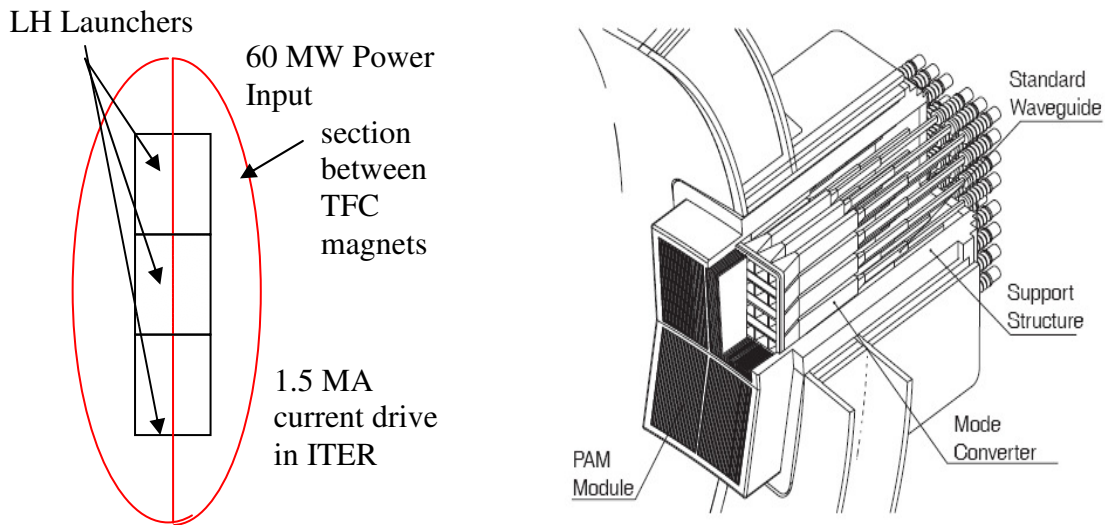


Figure 24: (a) LH Port Geometry⁵¹, (b) LH Launcher⁵¹.

Table 14: GCFTR-3 H&CD properties^{51,52,53}.

Property	GCFTR-3	ITER
Bootstrap Current	2.5 MA	~ 7.5 MA
Fractional Bootstrap Current	25%	$\sim 50\%$
Plasma Current	10 MA	15 MA
Maximum Simultaneous H&CD power	100 MW	110 MW
Total H&CD Capacity	120 MW	130 MW
Number of Port Plugs	6	10*
Power Density	33 MW/m ²	9.2 MW/m ² **

* 4 equatorial, 3 upper, 3 NBI, ** Power density in generic 20MW port

Since LH H&CD systems are currently the least efficient for heating, it is important to consider a secondary system. As LH systems are the most effective at driving current, an integral component for GCFTR-3 operation, the secondary system will not satisfy the required specifications with current or near-term technology. However, until research either improves LH heating efficiency or improves the current drive performance of the other two main systems, a secondary H&CD capability must be considered.

The most promising H&CD system in terms of plasma heating is the ICRH system. However, as ICRH H&CD systems only provide 0.15×10^{-20} A/Wm⁻² of current drive compared to $2-3 \times 10^{-20}$ m⁻³A/W in LH systems, more development is needed before the ICRH wave can fulfill GCFTR-3's requirements for steady-state operation. Another challenge in implementing ICRH H&CD systems is their large size. The ICRH launchers deliver a power density of 9.2 MW/m² compared to 33 MW/m² for LH launchers. The larger ICRH launchers would still be able to fit in between the magnets at the plasma chamber-reactor interface, but the shielding for the magnets would have to be significantly reduced. A launcher redesign would have to be completed to accommodate ICRH heating and reduced shielding. However, a backup ICRH system could be realized with reasonable improvements in performance.

D. Superconducting Magnet System

The GCFTR-3 magnet system is directly based upon the ITER^{54,55} design. The magnet system consists of three main sets of magnets: the central solenoid (CS), the toroidal field coils (TFC), and the poloidal field coils (PFC). Each of these systems can be seen in Figure 1. Only the first two systems will be discussed. The previous GCFTR-2 design³ has set some preliminary values for the magnet systems. These values must be revised as the GCFTR-3 will use an increased plasma current of 10 MA.

The CS for the GCFTR-3 is directly adapted from ITER and uses a cable-in-conduit Nb₃Sn conductor surrounded by an Incoloy 908 jacket. The superconductor is cooled through a channel carrying super-cooled Helium in the center of the cable-in-conduit. The CS creates a magnetic flux that inductively starts the plasma current and ohmically heats the plasma. It operates with a maximum magnetic field of 13.5 T. The two main dimensions of the CS are the flux core radius and the thickness. These two

factors are constrained by the amount of inductive start up Volt seconds needed, and by the maximum allowable stress in the CS, respectively. A goal of this project was to leave the size of the GCFTR-3 the same as the previous design, the GCFTR-2. The GCFTR-2's dimensions were analyzed to see if they could meet the new requirements of the GCFTR-3. This constrained the total flux core radius plus thickness of the CS not to exceed 1.36 m. The increase in plasma current to 10 MA forced the requirement for the inductive start Volt-seconds, VS_{start} , to increase from the previous design value based on 8.3 MA of plasma current. The required VS_{start} was a minimum of 107.3 Volt-seconds found using the IA code, which can be found in the Appendix D. VS_{start} was constrained using the following equation⁴³:

$$\pi \cdot \Delta B_{OH} \cdot R_v^2 \left[1 + \frac{\Delta_{OH}}{R_v} + \frac{1}{3} \cdot \left(\frac{\Delta_{OH}}{R_v} \right)^2 \right] \geq VS_{req-start}$$

where $\Delta B_{OH} \cong 2 \cdot B_{OH}^{max} = 27$ T, R_v is the flux core radius in meters, and Δ_{OH} is the thickness of the CS. A configuration of a flux core radius of 0.88 m and a CS thickness of $\Delta_{OH} = 0.48$ m created a VS_{start} of 108 V-s, satisfying the minimum needed, as well as leaving the total radius at 1.36 m. The stress in the CS was approximated using the following equation⁴³:

$$\sigma = C \cdot \frac{1}{f_{structure}} \cdot \left(\frac{B_{OH}^2}{2 \cdot \mu} \right) \cdot \left(\frac{R_v}{\Delta_{OH}} + \frac{1}{3} \right)$$

where C is a scaling constant equal to 1.4, μ is the permeability constant, $B_{OH} = 13.5$ T is the maximum magnetic field in the CS, and $f_{structure}$ is the volume fraction of the conductor. The $f_{structure}$ constant was calculated by determining the volume fraction of structural material in the conductors to the volume of the entire conductor as set by the original GCFTR design. The conducting strands have an internal diameter of 38 mm of conducting material and coolant chamber, surrounded by a 51 mm square of structural Incoloy 908. The value of $f_{structure}$ is 0.564. The maximum stress allowable in the CS solenoid, by ITER standards and Incoloy 908 limitations, is 430 MPa⁵⁵. When using a flux core radius of 0.88 m and thickness of 0.48 m, the stress created is about 399.9 MPa. This is very close to the limit; therefore any increase in plasma current above 10 MA would require a thicker CS to reduce the stress.

The toroidal field coils (TFCs) are designed using ITER⁵⁴ as a basis. The GCFTR-3 uses a Nb₃Sn cable-in-conduit superconductor with an Incoloy 908 jacket for support, as ITER does. These are also cooled through a channel carrying super-cooled helium in the center of the cable-in-conduit. The GCFTR-3 will only use 16 TFCs to create the toroidal magnetic field for the plasma. The thickness of the TFC for GCFTR is determined by conserving the tensile stress calculated in the same manner for the ITER TFC. The tensile stress is approximately equal to the magnetic force/cross section area or $s=F/A=(C* I_{TF}^2/A)$. Keeping the stress constant, the area of the GCFTR-3 TFCs is found when the ITER parameters⁵³ of a coil current of 9.13 MA and area of 0.3 m² are used. The TF coil current needed in the GCFTR-3 is calculated using Ampere's Law:

$$I_{TF} = \frac{B \cdot 2 \cdot R}{\mu_0 \cdot N}$$

where B is the magnetic field at the conductor, R is the radius at the conductor, and N is the number of TFCs. The magnetic field on the major axis of the plasma is related to the magnetic field at the TF conductor by⁴³:

$$B = B_{TFC} \left(\frac{R_v + \Delta m}{R} \right)$$

where B_{TFC} is the maximum magnetic field in the TFCs, R_O is the major radius, and Δm is the radial thickness of the CS and TFC. This magnetic field is calculated so that the current inside the conductor can be calculated. From this current we are able to calculate the required area by keeping the stress constant from ITER. Using these equations the area of the TFCs for the GCFTR-3 comes out to 0.1567 m². Keeping the radial thickness of the TFCs the same as the previous design of 0.43 m requires the TFCs to have a new width of 0.3645 m in the toroidal direction. The new width of the TFCs was checked and approved using a CAD model to make sure that 16 TFCs would fit around the CS without overlap.

In conclusion, the magnet system of the GCFTR-3 is based on a scaling down of ITER and the GCFTR-2 designs. The increase in plasma current from 8.3 to 10 MA required an increase in flux core radius to 0.88 m to acquire an adequate start-up V-s. The thickness of the CS coil was reduced to 0.48 m to conserve the size of the GCFTR-2 design. This thickness creates stresses in the CS very close to that of the maximum

allowed in the ITER design, but is within the limit. The area of the TFCs needs to be greater than originally allowed in the GCFTR-2 design due to the increase in plasma current. In order to keep the radial thickness of the TFCs constant at 0.43 m, the width was increased to 0.3645 m. This new width still allowed 16 TFCs to surround the CS.

VII. FUEL CYCLE

A. Objective

The goal of the GCFTR is to achieve a “deep-burn” (>90%) transuranic (TRU) burnup, if possible without the reprocessing of the fuel in the TRISO coated fuel particles. The TRU, whose composition is given in Appendix E, comes from LWR spent fuel³. The goal is to reduce the actinide inventory so as to decrease the need for high-level-waste (HLW) repositories of spent nuclear fuel such as Yucca Mountain. Previous studies^{3,4,7} indicate that this “deep burn” is feasible via the use of repeated cycling of the TRU with reprocessing and adding more fissile TRU to keep the k_{eff} of the system above about 0.8. Without reprocessing, the negative reactivity penalty introduced by the buildup of fission products and transmutation of fissile material would limit the practical burnup to approximately 15% with a 200 MW limit on the fusion power, and hence on the strength of the fusion neutron source⁷. Two approaches to extend the burnup of the TRU from spent nuclear fuel in GCFTR-3 without reprocessing are reported in this paper—1) lengthening the achievable fuel cycle by increasing the fusion neutron source strength to compensate a larger reactivity decrement (section VI) and 2) admixing ²³⁸U with the TRU in order to continuously produce TRU to reduce the reactivity decrement. With the addition of ²³⁸U in the fuel to produce TRU, the quantification of the “deep burn” goal becomes less clear cut, and the concept of “uranium utilization” (how much of the energy content of the original uranium is utilized to produce electricity) may be a better characterization of the objective.

B. Fuel Batching

In keeping with previous GCFTR fuel cycle analyses^{3,4,7}, the reactor core has been divided up into five equal volume annular regions. For the purposes of this analysis, each region is assumed to contain a uniform but time-dependent material composition throughout. Several shuffling patterns have been previously analyzed⁷,

though this report will focus on the “out-to-in” pattern. The first five reactor cycles for a new reactor starting up and utilizing this concept are shown in Fig. 25. Initially, fresh fuel is placed into all five core regions and this configuration is burned for one cycle. At the conclusion of the first cycle, the fuel assemblies in the region closest to the fusion source are removed, all other assemblies are shifted one region inward, and a batch of assemblies with fresh TRU fuel is introduced into the outermost region. This process is repeated for three subsequent cycles until a configuration is obtained (last row in Fig. 25) in which at beginning of cycle the outermost region contains fresh fuel, the adjacent region contains once-burned fuel, the next region contains twice-burned fuel, the next region contains thrice burned fuel and the innermost region contains four times burned fuel. Subsequent cycles would be identical to the cycle indicated by the fifth row in the figure, which is referred to as the “steady-state” cycle. This “5-batch, once-through” fuel cycle is the basis of the analysis in this section.

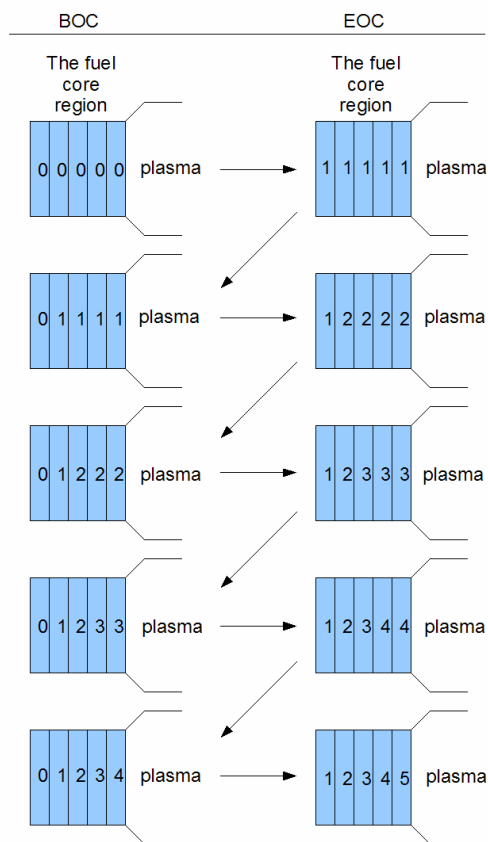


Figure 25: Approach to Steady State Fuel Cycle

Previous studies^{3,4,7} have primarily focused on fuel cycles involving recycling and reprocessing of TRU fuel in order to achieve burnup goals. In contrast, this work focuses on the potential of a once-through cycle to achieve a significant burnup of actinides. The term once-through designates a fuel cycle in which an assembly will be irradiated once in each of the five regions of the reactor, at which point in time it will be permanently removed from the reactor. The total irradiation time experienced by an assembly is therefore five times the length of a single operating cycle, and this total irradiation interval will be referred to as the residence time of an assembly. After removal, an assembly may be designated for disposal in a permanent repository or it may be recycled further in a different reactor, but it will not return to the GCFTR.

C. Methodology

In order to conduct the analysis, the TRITON⁵⁶ and EVENT³⁵ codes were implemented. EVENT is a deterministic neutron transport code which is used in the determination of the multiplication factor of the system and in producing the neutron flux distributions. TRITON is a code which couples a deterministic transport solver with the depletion code ORIGEN-S¹⁶. It was used to simulate the irradiation of the actinide fuel to determine variations in the material composition over time. The CSAS⁵⁷ sequences were used in order to create cross section libraries for use by EVENT. Although the SCALE package is primarily used in the analysis of thermal reactors, the use of the 238 group library provides the capability to treat fast spectrum assemblies as well. All analyses performed on collapsed spectra were collapsed from this 238 group library based on realistic energy distributions calculated for the GCFTR.

To conduct an initial depletion, the power distribution across each of the 5 annular regions was assumed to be flat (i.e. each produced 20% of the power). The TRITON code was implemented, depleting the TRU fuel based on a simplified pin cell geometry which recalculates the energy distribution of the flux approximately 4 times per operating cycle as it depletes the fuel. This calculation was performed for the entire residence life (five operating cycles) of a fuel assembly. The calculated 238 group spectra (Fig. 12) were automatically collapsed to the 3 groups that ORIGEN uses for the burnup calculation. Cross sections were then created for EVENT using a series of SCALE modules and collapsed from 238 groups to 27 groups (using a modified LMFBR

spectrum with a 14 MeV tail). In the EVENT model the materials were placed in the core in the reference out-to-in shuffle pattern, where for this case the composition of fresh fuel was placed in the outermost region, the composition after one cycle was placed in the second region, after two cycles in the third region, etc. At this point the compositions are only a rough estimate because of the starting assumption of a flat power distribution. A fixed-source EVENT run, with the fusion neutron source modeled as a volumetric source located throughout the plasma, was performed and the resulting flux profile was obtained for both beginning and end of cycle conditions. It was then assumed that the power distribution in the core would be proportional to the flux distribution. While the power distribution is actually proportional to the sum over groups of the product of the macroscopic fission cross section and the group flux in each region, this assumption is a reasonable approximation as long as the energy dependence of the fission cross sections is not highly spatially dependent. Proceeding with this approximation, the relative magnitudes of the fluxes for a new burnup history for the fuel was created. The original depletion calculation was repeated, but now instead of assuming a constant power over the residence time, the new power distribution obtained from EVENT is used. The average power that is experienced by an assembly over its residence remains the same, only it is now burned at a variable power throughout its life. The rest of the calculation was carried out in exactly the same manner with the new fuel compositions for the second pass through the procedure. This process was repeated until the compositions resulting from subsequent passes show little variation.

D. Cycle Length

It has been shown⁷ that a burnup of 90% FIMA cannot be achieved in a once-through cycle without a fusion neutron source that is larger than has been used in previous GCFTR designs (200 MW). Therefore, this analysis was intended to identify the maximum burnup that can be achieved within a single (5-batch) residence time in a steady-state (row 5) fuel cycle, while adhering to the restrictions given by the fusion neutron source as described in section VI. The minimum multiplication factor that can be accepted is primarily dependent on the strength of the fusion source supplying neutrons to the system. As argued in section IV, a fusion source of 200 MW will allow a thermal output of 3000 MW to be sustained at a k_{eff} value as low as around 0.8. Increasing the

fusion source to 500 MW, which was supported by the analysis in section VI, would allow for operation at 3000 MWt fission power at a subcritical multiplication factor of about 0.5.

In a steady-state cycle (row 5 in Fig. 25), fuel is present in the reactor at BOC that has already been irradiated for one, two, three and four burn cycles. Thus, lengthening the fuel cycle means that all previously burned fuel will have been burned longer and hence will be less reactive, resulting in a lower k_{eff} of the reactor as a whole. In order to maximize burnup in this once-through 5-batch cycle, it is necessary to determine the cycle length for which the end of cycle k_{eff} is at the lower limit that can be sustained by the fusion neutron source. It should be noted that the cycle length which can be sustained in a once-through cycle for pure TRU fuel is longer than that for an equilibrium cycle without reprocessing⁷ because less reactive fuel that had been burned more than five times would be present in the equilibrium fuel cycle. As is illustrated in Fig. 26, as TRU is irradiated not only does the primary fissile material, plutonium-239, deplete but neutron poisons such as plutonium-240 accumulate. This means that any equilibrium fuel cycle will inevitably tend towards a less reactive composition, resulting in a shorter operating cycle for a given limit on k_{min} ⁷.

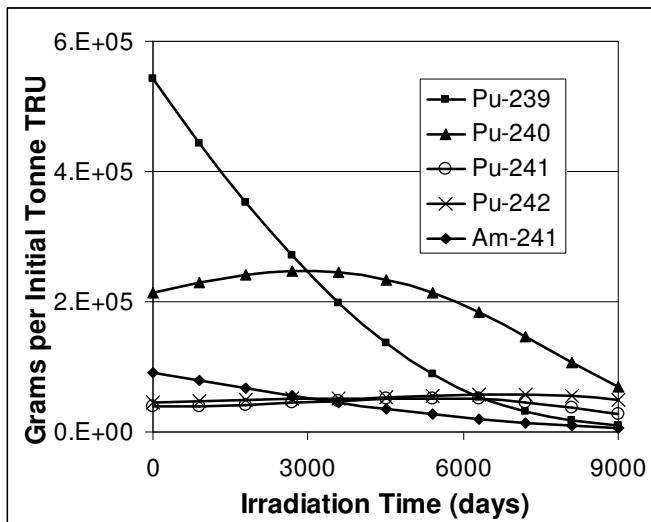


Figure 26: TRU Isotopic Composition for P≈86 MW/MTHM

The same basic steady-state fuel cycle calculation described above for a 600 day cycle length was repeated for cycle lengths of 1200, 1800 and 2400 days. Table 15 provides a comparison of several pertinent parameters for each of the cycle lengths analyzed. As discussed earlier, increasing cycle time not only increases the decrement in the k_{eff} over the course of a cycle, it also decreases the BOC k_{eff} that can be achieved and thus places a larger burden on the fusion source over the entire length of the cycle.

Table 15: GCFTR-3 Steady-State Fuel Cycle Parameters for Different Cycle Lengths

Parameter	Units	Cycle Length			
		600 Day	1200 Day	1800 Day	2400 Day
Thermal Power	MW	3000	3000	3000	3000
Cycles per Residence Time		5	5	5	5
5 Batch Residence Time	Years	8.2	16.4	24.7	32.9
BOC k_{eff}		0.987	0.917	0.856	0.671
EOC k_{eff}		0.927	0.815	0.714	0.611
BOC P _{fus}	MW	13	83	144	329
EOC P _{fus}	MW	73	185	286	389
TRU BOC Loading	MT	37	37	37	37
TRU Burned per Year	MT/FPY	1.12	1.12	1.09	1.05
TRU Burned per Residence	MT	9.2	18.4	26.8	34.7
TRU Burned per Residence	%	24.9%	49.7%	72.4%	93.7%
SNF Disposed per Year	MT/FPY	100.8	100.7	97.7	94.9
Average Core Flux Across Cycle	n/cm ² -s	5.91E+14	7.09E+14	8.67E+14	1.01E+15
Average Fast (>0.1 MeV) Flux	n/cm ² -s	2.66E+14	3.26E+14	3.90E+14	4.15E+14
Fluence per Residence Time	n/cm ²	1.53E+23	3.68E+23	6.74E+23	1.05E+24
Fast (>0.1 MeV) Fluence per Residence	n/cm ²	6.89E+22	1.69E+23	3.03E+23	4.31E+23

From this analysis, it appears that the availability of a fusion neutron source on the order of 500 MW would greatly enhance the burnup capability of a once-through transmutation cycle, though other issues begin to arise with these longer fuel cycles. As the operating k-effective is allowed to decrease, the location of the peak flux within the reactor core begins to shift radically towards the fusion source as illustrated in Fig. 27. In the case of a 2400 day cycle, the flux is peaked dramatically towards the plasma region, producing a peak to average ratio of almost 2.3, which is probably unacceptable. Examination of conventional methods (fuel zoning, burnable poisons, etc.) to reduce

power peaking is beyond the scope of this study, but it can be anticipated that such measures could reduce the power peaking to an acceptable value.

Thus, it seems likely that the burnup goal of >90% FIMA could be achieved in a once-through fuel cycle without reprocessing, provided of course that the TRISO fuel particles and cladding could survive the radiation damage associated with a fast neutron fluence of $> 4 \times 10^{23} \text{ n/cm}^2$.

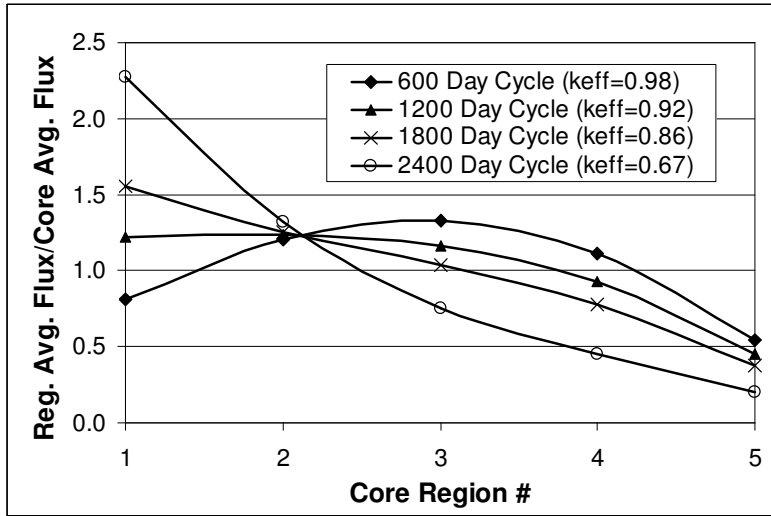


Figure 27: BOC Radial Flux Distribution

E. Fertile Admixing

In order to prevent the drop in the multiplication factor that results from a deep burnup of the fuel, the possibility of admixing fertile material in the form of U-238 with the normal TRU fuel composition was considered. Although the presence of fertile material initially displaces fissile material, the potential slower decrement in k_{eff} that would be experienced due to breeding of new fissile material might offset this adverse effect.

The primary analysis concerning the admixing of fertile material was performed for an infinite lattice of TRU fuel pins over a wide range of fertile concentrations. For the results shown in Fig. 28, each case contains the same overall mass of heavy metal (TRU + ^{238}U) and the fertile additions listed represent weight percentages ($M_{238}/(M_{238} + M_{\text{TRU}})$). Furthermore, the multiplication factor is calculated for an initial composition of

entirely fresh fuel that is depleted uniformly throughout the irradiation time. Since system leakage will not be significantly altered by changes in fuel composition, the trends exhibited by the value of k_{inf} should be representative of trends in the k_{eff} value for a whole reactor. While intuitively it seems as though any addition of fertile material would result in a reduced decrement in the multiplication factor over a given time interval, this behavior is not readily observable until a fertile concentration of nearly 70% is reached. At this concentration the infinite multiplication factor for the system is less than 0.8, which would require a fusion neutron source with more than 200 MW fusion power.

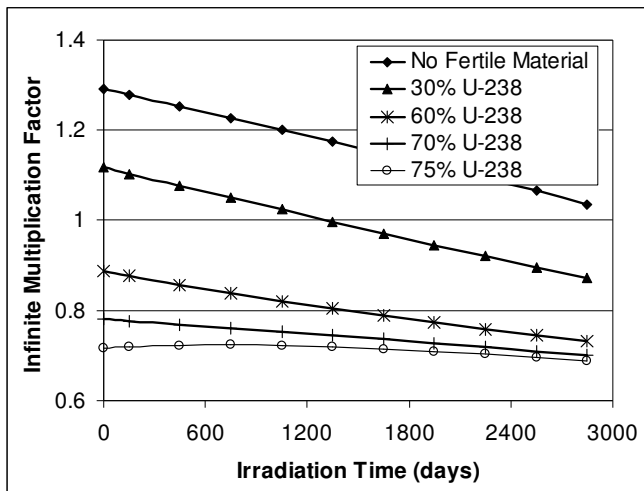


Figure 28: Infinite Lattice Multiplication Factor

With the addition of fertile material that is transmuted into TRU, it is no longer possible to characterize “deep burn” in terms of TRU burnup, as described before. Instead, the net TRU destruction, which will be defined as the percentage drop in the mass of actinides excluding uranium, will be used. This definition takes into account the reduced effectiveness of transmutation due to production of new actinides in the fertile material, but also the increased utilization of the potential energy content of the uranium. Although fertile material addition does reduce the decrement in the multiplication factor, the result is a significantly lower rate of actinide destruction as illustrated in Fig. 29.

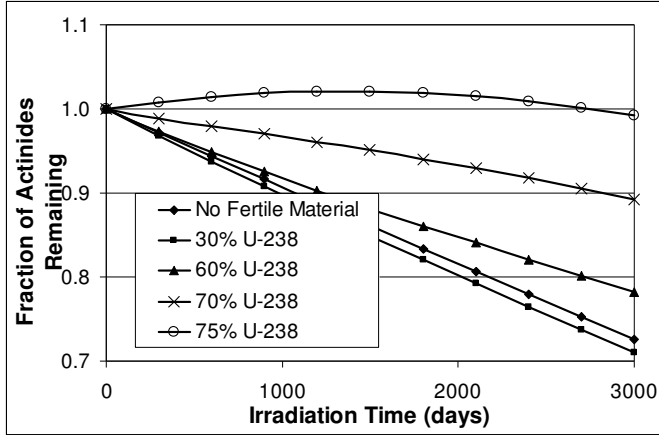


Figure 29: Fractional Burnup of Non-Uranium Actinides

Looking at the goal of the GCFTR-3 as resource utilization, instead of actinide destruction, suggests that the fractional burnup of the initial TRU + ^{238}U in the fuel is a more meaningful performance measure. This quantity is plotted in Fig. 30.

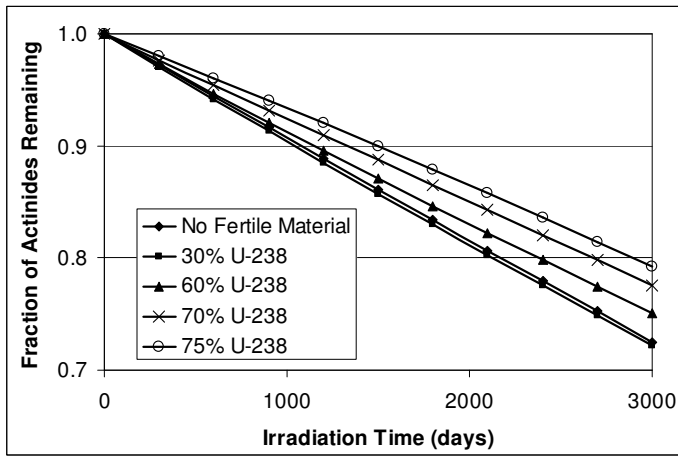


Figure 30: Fractional Burnup of TRU + ^{238}U

The addition of fertile material to the TRU fuel results in several pros and cons in terms of the overall goals of the GCFTR as a transmutation reactor. Due to the breeding taking place in the fertile material, the rate of drop in the k_{eff} is significantly lower at high fertile concentrations than with no fertile material present. This trend presents the potential for designing longer fuel cycles for neutron sources with $P_{\text{fus}} \leq 200 \text{ MW}$ than

would be achievable without fertile admixing. Table 16 provides a comparison of design parameters for two fuel cycle lengths and two fertile admixed compositions.

Table 16: Steady-State Fuel Cycle Parameters with Fertile Admixing

Parameter	Units	A	B	C	D
Cycle Length	Days	600	600	1800	1800
Fertile Admixing		None	70% U-238	None	70% U-238
5 Batch Residence Time	Years	8.2	8.2	24.7	24.7
BOC k_{eff}		0.987	0.590	0.856	0.577
EOC k_{eff}		0.927	0.576	0.714	0.534
BOC P_{fus}	MW	13	410	144	423
EOC P_{fus}	MW	73	424	286	466
TRU-U BOC Loading	MT	37	37	37	37
Non ^{238}U Actinide BOC Loading	MT	37	11.1	37	11.1
TRU-U Burned per Year	MT/FPY	1.12	1.17	1.09	1.12
Non ^{238}U Actinides Burned	MT/FPY	1.12	0.15	1.09	0.24
TRU-U Burned per Residence	%	24.9%	25.9%	72.4%	74.6%
Non ^{238}U Actinides Burned per Res.	%	24.9%	10.8%	72.4%	16.0%

Due to the large amount of fertile material that must be added in order for the benefit to be obtained, there is a large reduction in the initial fissile inventory and therefore a much lower multiplication factor for the system. In addition, there is a lower net TRU destruction rate due to the significantly lower TRU loading. These factors provide significant obstacles in the feasibility of this concept as an actinide burner, but indicates its promise for improving uranium resource utilization.

VIII. SUMMARY AND CONCLUSIONS

The fourth in a series^{3,4,7} of investigations of achieving “deep burn” of TRU from SNF by using it in coated TRISO particles to fuel sub-critical, gas-cooled fast reactors driven by tokamak fusion neutron sources has been described. The overall study was organized into related studies in the fuels, nuclear, thermal, neutron source and fuel cycle areas.

Objectives of the study in the fuels area were 1) to design a TRISO particle with better probability of survival in a fast flux, 2) to choose a reference fuel pin clad material to support the deep burn mission, 3) to design the fuel fabrication system, and 4) to

design a reprocessing system for TRISO fuel particles in the event that a reprocessing fuel cycle is required to achieve deep burn. The fuel pin design consisted of TRISO particles in a SiC matrix clad with ODS martensitic steel, with the TRISO particles having a reduced size TRU-oxide kernel surrounded in turn by a ZrC buffer layer, a WC layer, a SiC structural layer and an outer WC layer. Reprocessing the TRISO particle by grinding it down and then using the UREX/TRUEX process was judged feasible, if not attractive.

Objectives of the study in the nuclear design area were 1) to accommodate ports for plasma heating and current drive power; 2) to achieve tritium self-sufficiency, 3) to achieve a negative fuel Doppler coefficient, 4) to enhance passive safety, and 5) to simplify the shield design. The resulting core design consisted of two symmetric 160 degree semi-annular core segments 1.1 m wide by 3 m high surrounding the tokamak plasma neutron source on the outboard. The core would operate with $k_{\text{eff}} \leq 0.95$, a negative Doppler coefficient and a negative coolant voiding reactivity worth. The semi-annular reactor and plasma were surrounded by a 15 cm Li_2O containing tritium breeding blanket, which in turn was surrounded by a 64.5 cm shield (steel, Ir, Cd, B_4C , WC, HfC). A toroidal, pressurized lithium-injection-module was located over the core to provide passive poison injection into the core in response to an excessive increase in temperature.

Objectives of the study in the thermal design area were 1) to confirm the heat removal from the new fuel pins and 2) to define a design that was passively safe against a LOCA. A LOCA analysis confirmed the previously identified³ need for an Emergency Core Cooling System (ECCS), and a passively activated, pressurized, toroidal He accumulator located either above or below the annular core segments was incorporated into the design. Fuel pin temperatures during a LOCA with ECCS were predicted to remain below the respective melting points, thus providing passive safety against the LOCA.

Objectives of the study in the fusion neutron source area were 1) to examine the possibility of extending the source strength beyond the previous^{3,4} $P_{\text{fus}} \leq 200\text{MWt}$ level without changing dimensions or exceeding the present plasma physics database, 2) to confirm the feasibility of adapting the ITER divertor design from water to He cooling, 3) to adapt the ITER heating and current drive system, and 4) to modify the superconducting

magnet systems designs to remain within the ITER stress limits when the fusion power was increased. It was judged feasible to extend the fusion neutron source strength up to 500 MWt by a 20 % increase in plasma current, without changing dimensions or magnetic field, without exceeding ITER magnet system stress limits, and without significantly exceeding the present ITER physics database. Detailed heat removal calculations indicated that the ITER divertor adapted to He coolant could handle surface heat loads up to at least 2 MW/m² without excessive pumping power requirements. A lower hybrid electromagnetic heating and current drive system to deliver up to 100 MWt heating power and drive 7.5 MA of plasma current was adapted from the ITER design.

Objectives of the study in the fuel cycle area were 1) to investigate “deep burn” fuel cycles that would achieve very high burnup of TRU-oxide fuels and 2) to investigate “high uranium utilization” fuel cycles that would extract very high fractions of the potentially available energy in TRU-U238-oxide fuels. It appears possible to achieve > 90% burnup of TRU-oxide fuel with near-term fusion neutron sources producing up to 400 MWt, without reprocessing, provided that the fuel can survive the associated radiation damage. It also appears possible to achieve similarly high burnup in cores loaded with 70% ²³⁸U-30% TRU fuel without reprocessing, using fusion neutron sources producing up to 500 MWt, again providing that the fuel can survive the radiation damage.

Thus, the overall conclusion of this study is that it is possible to design a passively safe, sub-critical GCFTR, with a 400-500 MWt tokamak fusion neutron source only slightly exceeding the present ITER design database, which can achieve $\geq 90\%$ burnup of the TRU-oxide or 70% ²³⁸U-30% TRU-oxide fuel in TRISO particles without the need to reprocess, if the fuel can withstand the radiation damage. If the fuel can not withstand the fast neutron fluence of 4×10^{23} n/cm² associated with 90% burnup, then it will be necessary to reprocess the fuel to achieve 90% burnup, and a less powerful neutron source will suffice.

APPENDIX A FUELS

Equations for Stress Analysis of Fission Product Gas Buildup

$$PV = nRT \quad (A.1)$$

P = pressure, V = volume, n = moles, R = gas constant, T = temperature

$$\sigma_{SiC} = \frac{P * r}{2 * t} \quad (A.2)$$

r = radius at inner surface of layer, t = thickness of layer

$$e = \frac{\sigma_{SiC} / E_{SiC}}{1 - \nu_{SiC}} \quad (A.3)$$

$$\sigma_{WC} = \frac{E_{WC} * e}{1 - \nu_{WC}} \quad (A.4)$$

e = elongation of SiC, E = Young's Modulus, ν = Poisson's Ratio

Burnup, Pressure, & Stress Chart

Time(days)	600	2400	4000	6000	10000	14000	18000	26000	30000
H	5.32E-12	1.71E-11	2.80E-11	4.23E-11	7.21E-11	1.08E-10	1.48E-10	2.39E-10	2.92E-10
He	7.60E-11	2.12E-10	3.05E-10	3.98E-10	5.26E-10	6.13E-10	6.78E-10	7.73E-10	8.10E-10
Br	2.42E-11	7.31E-11	1.06E-10	1.35E-10	1.56E-10	1.52E-10	1.38E-10	1.08E-10	9.44E-11
Kr	4.61E-10	1.31E-09	1.87E-09	2.46E-09	3.31E-09	3.88E-09	4.30E-09	4.90E-09	5.12E-09
I	4.47E-10	1.14E-09	1.57E-09	1.92E-09	2.18E-09	2.18E-09	2.08E-09	1.81E-09	1.67E-09
Xe	7.97E-09	2.21E-08	3.09E-08	4.00E-08	5.31E-08	6.22E-08	6.89E-08	7.87E-08	8.23E-08
Totals (moles)	8.99E-09	2.49E-08	3.48E-08	4.49E-08	5.94E-08	6.91E-08	7.63E-08	8.65E-08	9.03E-08
nRT	7.04E-05	0.000195	0.000272	0.000352	0.000465	0.000541	0.000597	0.000677	0.000707
Volume (m ³)	1.95E-11	1.95E-11	1.95E-11	1.95E-11	1.95E-11	1.95E-11	1.95E-11	1.95E-11	1.95E-11
Pressure (MPa)	3.60	9.97	13.93	18.00	23.80	27.69	30.56	34.66	36.18
Burnup (%)	7.41	19.56	27.15	35.28	46.88	54.85	60.81	69.57	72.92
Stress SiC (MPa)	6.93	19.16	26.79	34.62	45.76	53.25	58.77	66.66	69.58
Stress WC (MPa)	12.77	35.33	49.39	63.83	84.37	98.18	108.35	122.89	128.28

ORIGEN was run to determine the buildup of gases. The volume is the amount of space within the buffer. Using the optimization equations, the stresses can be calculated.

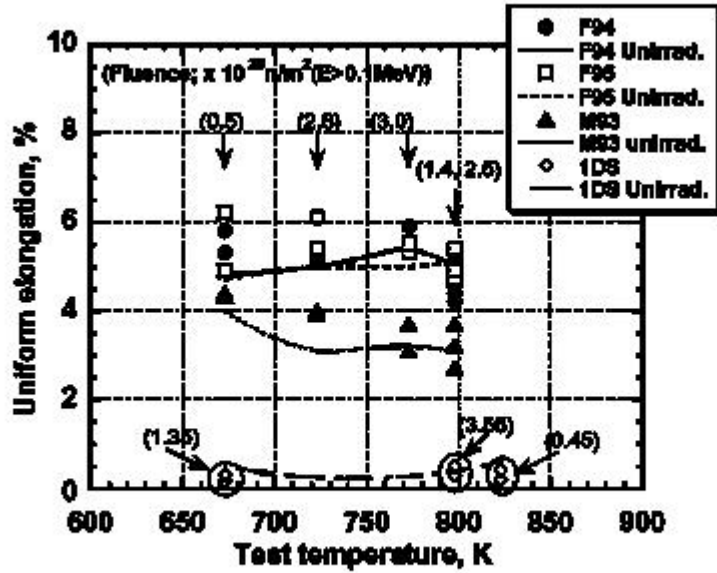


Figure A.1 Uniform elongation of ODS ferritic/martensitic steel claddings before and after irradiation²⁰

APPENDIX B NUCLEAR

1. Effect of Depletion on Multiplication Constant

The fuel will be burned five times, in different annular locations, as discussed in Section VII. In order to gain some insight into the effect of fuel depletion on the range of the multiplication constant, a series of calculations was made for the pure TRU fuel. In these calculations, the fuel was uniform throughout the core, was not shuffled, and was uniformly depleted at 3000 MWth over 600 day intervals, using ORIGEN. The multiplication constant was calculated for the fresh fuel and after each 600 day depletion interval, using both the EVENT 3D model and MCNP 3D model, both with cross sections at 300K. The results in Table B.1 provide some indication of the effect of TRU depletion and fission product buildup on the multiplication constant (calculations with fuel shuffling are discussed in section VII), as well as providing a comparison between the 3D, multigroup EVENT P_1 and the 3D, continuous energy MCNP calculations.

Burned Time (days)	K_{eff} @ 300K (MCNP)	K_{eff} @ 300K (EVENT P_1)
0	1.03505	1.02480
600	0.91491	1.00320
1200	0.87167	0.96109
1800	0.82811	0.90641
2400	0.78247	0.85196
3000	0.73586	0.80816

Table B.1: 3D K_{eff} vs. Burnup for Uniform Core Depletion

2. Power Distribution

Figures B.1 below displays the flux profiles of the annular reactor core with and without the 20° sectors removed. As was stated in Section IV, the multiplication constant does not significantly decrease with the removal of the fuel. The only significant change with this design is the necessity for shielding around the Heating and Current Drives that are fed through the toroidal magnets and removed fuel regions.

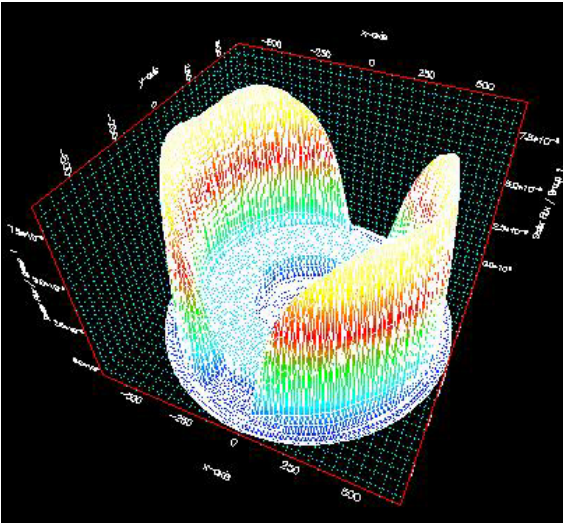
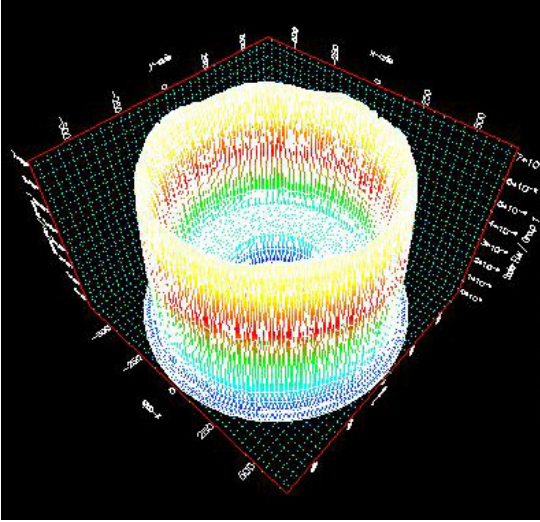


Figure B.1: Flux distribution of entire core without removed sectors and with 20° removed

APPENDIX C THERMAL

1. Core Thermal Analysis

A general thermal circuit equation for the particular case in this study is as follows:

$$T_{FM} - T_{\infty} = \frac{q''' D}{2} \left(\frac{D}{4k_f} + \frac{g}{k_g} + \frac{c}{k_c} + \frac{1}{h} \right) \quad (C.1)$$

where:

T_{FM} is the temperature at the middle of the fuel pin

T_{∞} is the temperature of the coolant

q''' is the volumetric heat generation rate

D is the diameter of the fuel pin

k_f is the conductivity of the fuel material

g is the gap thickness

k_g is the conductivity of the gap

c is the clad thickness

k_c is the conductivity of the clad

h is the heat transfer coefficient of the coolant

2. Evaluation of He Flow Rates

For evaluation of Helium flow rates from heat discharge.

Reynolds number: $Re = \rho * v_{avg} * D_e / \mu$

Rho = density

D_e = hydraulic diameter

Mu = fluid viscosity

Prandtl number: $Pr = \nu / \kappa$ (viscosity / thermal diffusivity)

Nu = viscosity

Kappa = thermal diffusivity

Turbulence is assumed to occur at $Re > 2300$

Laminar case (natural convection):

$$Nu_{lam} = 0.664 * Re^{1/2} * Pr^{1/3}$$

Turbulent case (forced convection):

$$Nu_{turb} = (0.037 * Re^{4/5} * Pr) / (1 + 2.443 * Re^{-1/10} * (Pr^{2/3} - 1))$$

$$Nu = h * D_e / k$$

$$Q'' = h * A * \Delta T$$

3. Determination of Clad Temperature During a LOCA

Known parameters:

- ◆ Decay Heat as a Function of Time
- ◆ Average Specific Heat of the Core
- ◆ Total Mass of the Core
- ◆ Initial Clad Temperature

Starting Clad Temp (Kelvin)	Core Mass (kg)	Effective Core Specific Heat (J / kg K)
831	6.00E+05	600

$$Q(t)_{core} = Q(t)_{decay} - Q(t)_{reject} = mc\Delta T \quad (C.2)$$

$$\text{Equation 2: } Q(t)_{reject} = 2.2 \left(\frac{T_{GCFTR-2}}{T_{PFR}} \right)^4 Q(t)_{reject_PFR} \quad (C.3)$$

Starting with the inner clad temp based on thermal analysis of the core, the first change in temperature was calculated from equation 1. The rejection heat of the GCFTR-2 was estimated by scaling the rejection heat from the PRF by a geometric factor and a factor based on the Stefan-Boltzman Law. The scaling factor was updated iteratively after one minute intervals at which time a new change in temperature was determined.

4. Accumulator Design

decay heat load → design heat transfer coefficient

- $Q_h = hA(\Delta T)$

design heat transfer coefficient → **Nusselt number**

- $Nu = hDh/k$

Nusselt number → **Reynold's number**

- $Nu = .023 Re^{0.8} Pr^{.33}$ (Dittus – Boelter correlation)

Reynold's number → design velocity

- $Re = \rho v_{bar}/\mu$

Design velocity → mass flow rate

- $\dot{M} = \rho Av$

Mass flow rate → **integral mass (accumulator design volume)**

- Left rectangular approx ($t1 \times \dot{m}$) summation; slightly over estimates volume

APPENDIX D FUSION NEUTRON SOURCE

1. Plasma Performance Code

The performance code uses a power balance methodology to solve for the performance parameters. Essentially the goal is to solve for the auxiliary using Equation (D.7). All other parameters are calculated from inputs. The code was written so that H-factor, normalized beta, and the current could be specified as variables. The basic equations are listed below⁴³.

$$P_{DT} = \frac{1}{4} (\bar{n}_{e20})^2 \langle \sigma v \rangle UV_p \quad (D.1)$$

$$P_{\alpha} = 0.2 P_{DT} \quad (D.2)$$

$$P_{brem} = 5.35 \times 10^{-3} (\bar{n}_{e20})^2 Z_{eff} \sqrt{T_{keV}} V_p \left(\frac{(1 + \alpha_N)^{1.5} + \sqrt{1 + \alpha_N + \alpha_T}}{1 + 2\alpha_N + 0.5\alpha_T} \right) \quad (D.3)$$

$$P_{loss} = \frac{W_{th}}{\tau_E} \quad (D.4)$$

$$\tau_E = 0.144 I^{0.93} B^{0.15} P^{-0.69} \bar{n}_{e20}^{-0.41} M^{0.19} R^{1.97} A^{-0.58} \kappa^{0.78} \quad (\text{D.5})$$

$$W_{th} = 0.024 T_{keV} \bar{n}_{e20} (1 + f_{ion}) V_p \quad (\text{D.6})$$

$$P_{aux} = P_{brem} + P_{loss} - P_\alpha \quad (\text{D.7})$$

$$P_{nwl} = \frac{0.8 P_{DT}}{A_{FW}} \quad (\text{D.8})$$

$$q_{FW}'' = \frac{(0.2 P_{fus} + P_{aux})(1 - f_{div}) \hat{f}_{FW}}{(2\pi R) \left(2\pi a \sqrt{\frac{1}{2}(1 + \kappa^2)} \right) (1 - \epsilon_{div})} \quad (\text{D.9})$$

$$q_{95} = \frac{5a^2 B_{coil}}{2RI} (1 + \kappa^2) (1 + 2\delta^2 - 1.2\delta^3) \frac{\left(1.17 - \frac{0.65}{R/a} \right)}{\left(1 - \frac{1}{(R/a)^2} \right)^2} \quad (\text{D.10})$$

$$B_0 = \frac{B_{coil}}{(R/a)} \left((R/a) - 1 - \frac{\Delta_{BS}}{a} \right) \quad (\text{D.11})$$

$$\bar{n}_{e20} = fGrnwld \frac{I}{\pi a^2} \quad (\text{D.12})$$

$$\beta_T = \frac{\beta_N I}{a B_0} \quad (\text{D.13})$$

$$B_p = \frac{I}{5a \sqrt{0.5(1 + \kappa^2)}} \quad (\text{D.14})$$

$$\Delta\Phi_{CS} = \left[1.256R \ln\left(\frac{8R}{a\sqrt{\kappa}}\right) + \frac{1}{2} \ln(1.65 + 0.89 * (q_{95} - 1)) - 2 \right] I + 1.256 C_{ejima} R I \quad (D.15)$$

$$f_{BS} = \left(1.32 - 0.235 \frac{q_{95}}{q_0} + 0.0185 \left(\frac{q_{95}}{q_0} \right)^2 \right) \left(\sqrt{\frac{1}{(R/a) \beta_p}} \right)^{1.3} \quad (D.16)$$

$$\gamma_{CD} = \frac{\bar{n}_{e20} R (1 - f_{BS}) I Q_p}{10 P_{fus}} \quad (D.17)$$

$\gamma_{CD} \equiv$ gamma efficiency of current drive

$f_{BS} \equiv$ fractional bootstrap current

$\Delta\Phi_{CS} \equiv$ required Start-up Flux for Central Solenoid (Volt/sec)

$\beta_p \equiv$ poloidal beata

$\beta_T \equiv$ toroidal beta

$\beta_N \equiv$ normalized beta

$\bar{n}_{e20} \equiv$ electron density divided by 1×10^{20}

$\kappa \equiv$ plasma elongation

$V_p \equiv$ plasma volume

$Q_p \equiv$ power amplification factor

$f_{ion} \equiv$ plasma ion fraction

$\alpha_N \equiv$ density scaling factor (<1)

$\alpha_T \equiv$ temperature scaling factor (<1)

$W_{th} \equiv$ thermal power (MJ)

$q_{FW}'' \equiv$ heat flux to the first wall (MJ/m²)

$P_{nvt} \equiv$ neutron flux to the first wall (MW/m²)

$T_{keV} \equiv$ plasma temperature (keV)

2. Analytical Approximation for Divertor Heat Removal

The analytical model was based on flow through a straight pipe of length L that is a distance below a surface subject to a uniform heat flux. It can be shown that if the

maximum surface temperature is assumed at the exit where the distance, t , between the tube surface and the incident surface is a minimum, Equation (D.18) describes the 1-D heat transfer shown in Figure D.1.

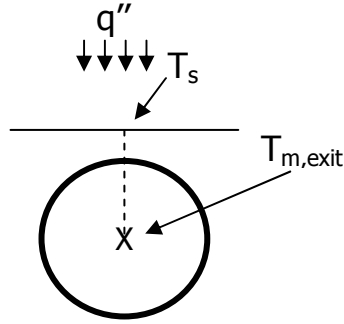


Figure D.1. Heat transfer model.

$$q'' = \frac{T_s - T_{m,exit}}{\left(\frac{1}{h_o} + \frac{t}{k}\right)} \quad (D.18)$$

To eliminate the exit temperature term since it is not known a priori, the conservation of energy is used for a control volume consisting of the tube within a block and treating helium as an ideal gas. Then combining Equations (D.18) and (D.19), the useful relation, Equation (D.20), is obtained.

$$Q = q'' Lw = \dot{m}c_p \Delta T$$

$$q'' = \frac{\dot{m}c_p \Delta T}{Lw} \quad (D.19)$$

$$q'' = \frac{T_s - T_{in}}{\left(\frac{DL}{\dot{m}c_p} + \frac{1}{h_o} + \frac{t}{k}\right)}$$

(D.20)

Where: L = tube length

D = tube diameter

t = minimum distance between tube surface and pipe surface

h_o = local convection heat transfer coefficient at the exit

The program used for this analysis was Engineering Equation Solver (EES). By knowing all variables of Equation (D.20), the mass flow rate was varied to obtain a heat flux value that satisfies the constraints. The local convective heat transfer coefficient at the exit was determined by computing the Reynolds number, Friction Factor using Colebrook Formula⁴⁸, and Nusselt Number using the Petukhov correlation⁴⁹ based on the given mass flow rate as shown below.

$$\text{Re} = \frac{\rho V D}{\mu} = \frac{\dot{m} D}{A_{x\text{-sec}} \mu} \quad (\text{D.21})$$

$$\frac{1}{\sqrt{f}} = -2.0 \log \left(\frac{\varepsilon/D}{3.7} + \frac{2.51}{\text{Re} \sqrt{f}} \right) \quad (\text{D.22})$$

$$\text{Nu}_D = \frac{\left(\frac{f}{8} \right) \text{Re} \text{Pr}}{1.07 + 12.7 \left(\frac{f}{8} \right)^{1/2} \left(\text{Pr}^{2/3} - 1 \right)} \quad (\text{D.23})$$

$$h_o = \frac{\text{Nu}_D k}{D} \quad (\text{D.24})$$

The results of the EES code run under similar input conditions as the 3-D Fluent calculations are shown in Figure D.2. The EES program used a straight length of 1.73 m.

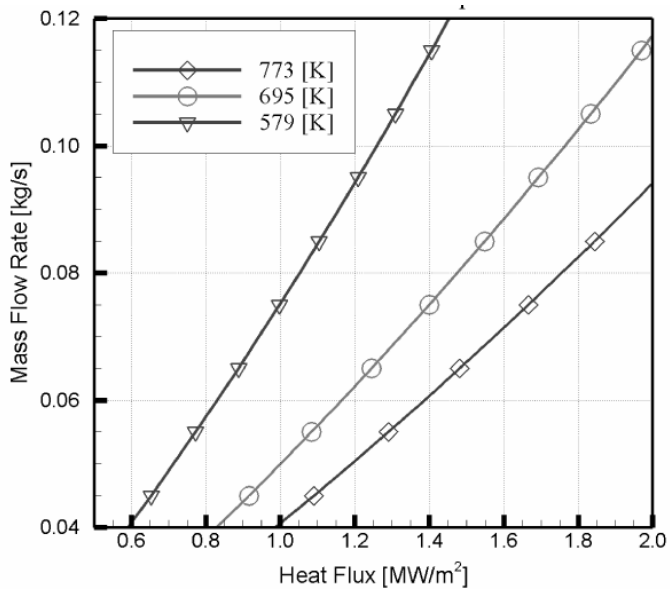


Figure D.2 EES Max temperature for outer vertical target.

For the case of the Center Dome target, a length of 2.53 m was used in the EES program. The results are shown in Figure D.3.

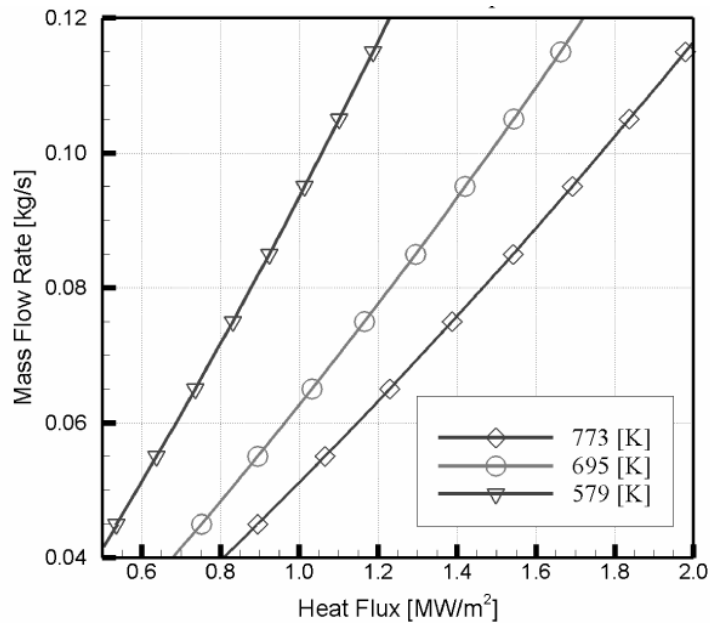


Figure D.3 EES Max temperature for center dome.

Figure D.4 shows the improved results for the center dome when multiplication factors of 2 and 4 were used to approximate the swirl tape.

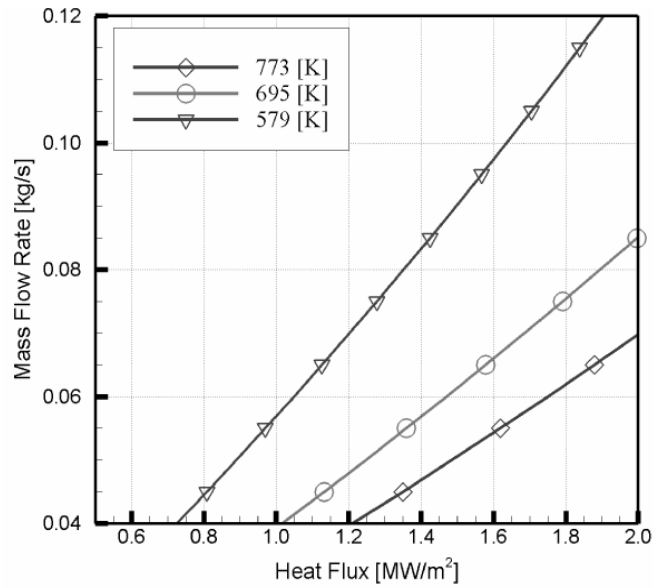


Figure D.4 EES Max temperature for center dome with swirl tape.

Figure D.5 shows the effect of the swirl tape enhancement factors on the outer vertical target.

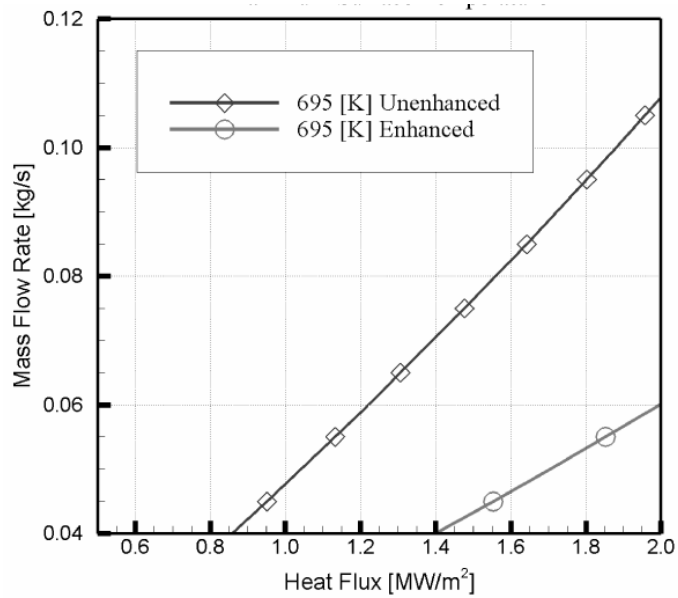


Figure D.5 EES Max temperature for outer target with swirl tape.

3. Additional Fluent Results

Figure D.6 shows the results of a contour map for the ratio of the pumping power to the total heat removed by the channel based on Fluent results.

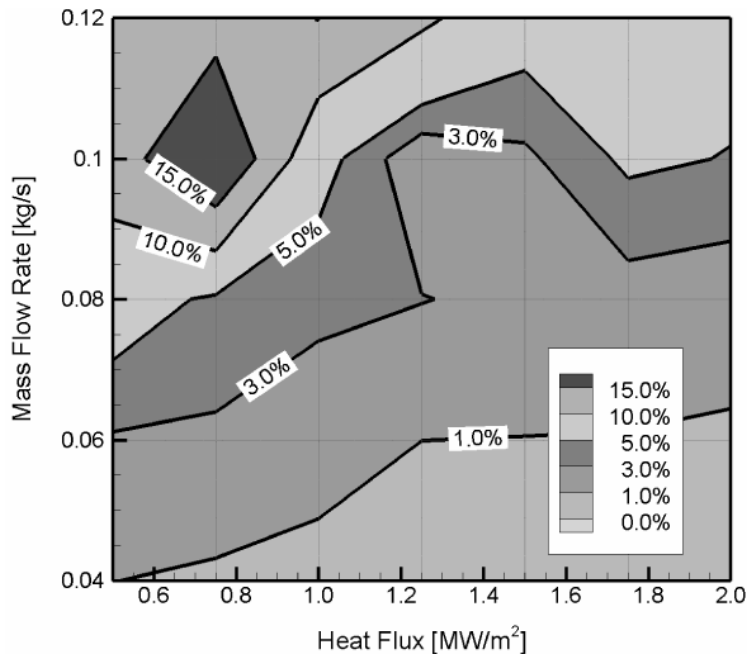


Figure D.6 Percentage of pumping power of total heat removed.

The operation within the temperature limit of 773 K is achievable for the analyzed heat flux range of 0.5 to 2 MW/m² within the 1% - 5% region. This could be decreased by using heat transfer enhancement methods such a swirl tape.

Recommendations for future work are to model the inner vertical target and dome, model the copper block with the CFC and tungsten tiles on the plasma-facing surface, then incorporate the swirl tapes in the cooling tubes, and finally to assemble the blocks matching the geometry of one entire divertor cassette.

4. H&CD Review

The foremost effect of H&CD systems is the power delivered in heating to the plasma. Electromagnetic waves that are in resonance with the ions and/or electrons in the D-T plasma deposit energy to the charged particles via Landau dampening⁵⁸. There are several important resonant frequencies associated with the heating of ions and electrons.

Three main radio-frequency H&CD systems are being researched and used today. They are systems that utilize the ion-cyclotron (ICRF), electron-cyclotron (ECRF), and lower hybrid (LHRF) resonances. These systems are employed in the Joint European Torus (JET)⁵⁹, and many other tokamaks, and will be implemented in ITER⁵¹.

In order to conduct electromagnetic waves at the resonance frequencies from the generators to the wave launcher/antenna, a waveguide must be employed. The size of the required transmission waveguides (from the generators to launchers) are related to the wavelength of the wave being transmitted. Because of the limited plasma access through the annular reactor in the GCFTR, this is a real constraint and concern. The lower the chosen resonant frequency, the larger the respective waveguide must be. This presents geometric complications in implementing an H&CD system.

Table D.1 Resonance Frequency Properties^{51,60}

Resonance	Ion Cyclotron	Electron Cyclotron	Lower Hybrid
Frequency	.055 GHz	170 GHz	5 GHz
Wavelength	5455 mm	1.765 mm	60 mm
Waveguide Dimension	280 mm (dia.)	50 mm (wide, corrugated)	107 mm (dia.)

The electron-cyclotron resonance frequency is very promising. The waveguide and launcher size is small compared to other H&CD options, making it attractive for use in GCFTR. ECRF H&CD also has a high current drive efficiency. However, the 170 GHz resonance frequency utilized in H&CD systems is very high, taxing our current wave-generation technological limits, which in combination with other expensive components such as diamond windows, makes ECRF H&CD systems very costly. Additionally, an optimum frequency for the electron-cyclotron H&CD is 250 GHz⁵⁹ which is currently unrealistic for generation purposes. ECRF H&CD is an attractive option for a space-constrained tokamak such as GCFTR.

The ion-cyclotron resonance frequency H&CD systems are well known and well researched. Because of the fusion community's familiarity with ICRF H&CD systems, they are always a viable option. They are utilized in JET and most tokamaks, and will be implemented into ITER in the combined H&CD system. ICRF H&CD systems are relatively inexpensive to make and are available with today's technology. However, they

have the lowest current drive efficiency and largest size of the three main H&CD systems. This lessens their value in a tokamak like the one employed in GCFTR, as both current drive and size are important parameters to maximize and minimize, respectively.

H&CD systems relying on the lower hybrid resonance frequency are the type utilized in this GCFTR design. The size of the LH waveguides and launchers is in between the ICRF and ECRF sizes, and the frequency of 5 GHz is more realistic than ECRF's 170 GHz. The most important attribute of LH H&CD systems is that they have the highest current drive efficiency of the three common H&CD systems, an important parameter for the high current GCFTR tokamak. An additional high power density and acceptable launcher size (Table D.2) make this system a good fit for GCFTR's requirements.

Table D.2 Parameters of H&CD Systems^{51,62-64}

Resonance	ICRF	ECRF	LH
Current Drive Efficiency	$0.15 \times 10^{-20} \text{ A/Wm}^{-2}$	$0.2 \times 10^{-20} \text{ A/Wm}^{-3}$	$2-3 \times 10^{-20} \text{ m}^{-3} \text{ A/W}$
Power Density	9.2 MW/m^2	$110 \text{ kW/cm}^2 @ 252 \text{ GHz}$	33 MW/m^2

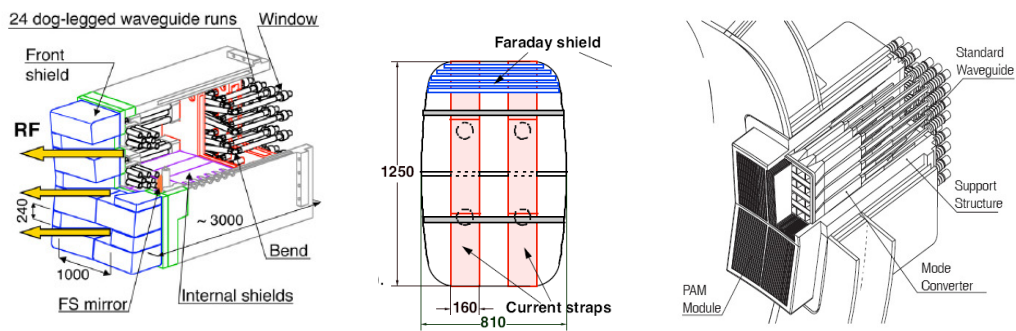


Figure D.7 Designs of 20 MW ITER launchers^{51,65,66} (a) ECRF (b) 1/2 ICRF (c) LH

Current drive is an important part of any H&CD system. It allows the plasma current to be kept high after the induced current from the central solenoid is no longer present. The driven current from a H&CD system must be sufficient to provide the plasma current not accounted for by the bootstrap current. A major research goal today is to design a tokamak with full (100%) bootstrap current drive.

APPENDIX E: FUEL CYCLE

Two different collapsed energy group structures were used in the calculations described in Section VII. Table E.1 shows the 27 group structure that was utilized for neutron transport calculations in the EVENT code and Table E.2 displays the 3 group structure that was employed in the depletion calculations within ORIGEN-S.

Table E.1: 27 Energy Group Structure for EVENT

Group	Max Energy (eV)
1	2.00E+07
2	6.43E+06
3	3.00E+06
4	1.85E+06
5	1.40E+06
6	9.00E+05
7	4.00E+05
8	1.00E+05
9	1.70E+04
10	3.00E+03
11	5.50E+02
12	1.00E+02
13	3.00E+01
14	1.00E+01
15	3.05E+00
16	1.77E+00
17	1.30E+00
18	1.13E+00
19	1.00E+00
20	8.00E-01
21	4.00E-01
22	3.25E-01
23	2.25E-01
24	1.00E-01
25	5.00E-02
26	3.00E-02
27	1.00E-02

Table E.2: 3 Energy Group Structure for ORIGEN-S

Group	Max Energy (eV)
1	2.00E+07
2	1.00E+06
3	6.25E-01

In Section VII, “fresh TRU” describes a fuel composition which is typical of light water reactor spent nuclear fuel that has undergone reprocessing to extract the uranium, leaving behind a distribution of actinides. The distribution of primary isotopes in this fresh TRU is shown in Table E.3.

Table E.3: Initial TRU Fuel Composition

Isotope	Mass %
NP237	4.34%
PU238	1.25%
PU239	54.10%
PU240	21.34%
PU241	3.89%
PU242	4.69%
AM241	9.23%
AM243	1.03%
CM244	0.12%

REFERENCES

1. W. M. Stacey, et al., "A Fusion Transmutation of Waste Reactor", *Fusion Sci. Technol.*, 41, 116 (2002).
2. A. N. Mauer, W. M. Stacey, J. Mandrekas and E. A. Hoffman, "A Superconducting Tokamak Fusion Transmutation of Waste Reactor", *Fusion Sci. Technol.*, 45, 55 (2004).
3. W. M. Stacey, et al., "A Sub-Critical, He-Cooled, Fast Reactor for the Transmutation of Spent Nuclear Fuel", *Nuclear Technol.*, to be published (October, 2006).
4. W. M. Stacey, et al., "A Sub-Critical, Gas-Cooled Fast Transmutation Reactor with a Fusion Neutron Source", *Nuclear Technol.*, 150, 162 (2005).
5. W. M. Stacey, J. Mandrekas and E. A. Hoffman, "Sub-Critical Transmutation Reactors with Tokamak Fusion Neutron Sources", *Fusion Sci. Technol.*, 47, 1210 (2005).
6. E. A. Hoffman and W. M. Stacey, "Comparative Fuel Cycle Analysis of Critical and Sub-Critical Fast Reactor Transmutation Systems", *Nuclear Technol.*, 144, 83 (2003).
7. J. W. Maddox and W. M. Stacey, "Fuel Cycle Analysis of a Sub-critical, Fast, He-Cooled Transmutation Reactor with a Fusion Neutron Source", *Nuclear Technol.*, submitted (2006).
8. <http://iter.org>
9. Long, et al., "Fabrication of ORNL Fuel Irradiated in the Peachbottom Reactor and Post-irradiation Examination of the Recycle Test Elements 7 and 4", Oak Ridge National Laboratory report (Oct. 1974).
10. D. A. Petti, et al., "Key Differences in the Fabrication, Irradiation and High Temperature Accident Testing of U. S. and German TRISO-Coated Particle Fuel, and Their Implications on Fuel Performance", *Nucl. Eng. Des.*, **222**, 281 (2003).
11. B. Kadomtsev, et al., "USSR Contribution to the Phase IIA INTOR Workshop", Vol 2, p. VIII-64 (1982).
12. M. Sawan, Univ. Wisconsin, personal communication (2004).

13. "Fuel Performance and fission product behavior in gas cooled reactors," IAEA-TECDOC-978.
14. W. Van Roojen, Delft Techn. Univ., personal communication, 2006.
15. K. Miller, et al. "Consideration of the effects of partial debonding of the IPyC and particle asphericity on TRISO-coated fuel behavior." *J. Nuc. Mater.*, 79-89, 334 (2004)
16. "ORIGEN-S: SCALE System Module to Calculate Fuel Depletion, Actinide Transmutation, Fission Product Buildup and Decay, and Associated Radiation Source Terms," NUREG/CR-200, Rev. & (ORNL/NUREG/CSD-2/V2/R7) Oak Ridge National Laboratory (2004).
17. M. Zhou, Georgia Tech, Personal communication, 2006.
18. J.T. Busby, Oak Ridge National Lab, personal communication, 2006.
19. S.T. Nozawa, et al., "Determining the shear properties of the PyC/SiC interface for a model TRISO fuel," *J. Nuc. Mater.*, 182-194, 350 (2006).
20. T. Yoshitake, et al., "Ring-tensile properties of irradiated oxide dispersion strengthened ferritic/martensitic steel claddings," *J. Nucl. Mater.*, 329-333, 344 (2004).
21. S. Ukai and M. Fujiwara, "Perspective of ODS alloys application in nuclear environments," *J. Nucl. Mater.*, 307-311, 749 (2004).
22. S. Ukai, et al., "R&D of oxide dispersion strengthened ferritic martensitic steels for FBR," *J. Nucl. Mater.*, 258-263, 1745 (1998).
23. S. Zinkle, "Advanced Materials for Fusion Technology," Oak Ridge National Lab, 20-24 Sep. 2004. April (2006).
24. R. Jones, "SiC^f/SiC Composites for Advanced Nuclear Applications," *Ceramic Engineering and Science Proceedings*, 24,4 (2003), 261.
25. NIST Property Data Summary for Silicon Carbide (SiC). 08 Feb. 2001. Ceramics Division, NIST. 02 May 2006. <http://www.ceramics.nist.gov/srd/summary/ftgsic.htm>
26. S. Ukai and M. Inoue, "ODS Steel Clad Mox Fuel-Pin Fabrication and Irradiation Performance in EBR-II," *Nucl. Technol.*, 138, 240 (2002).

27. H. Bairiot and G. VanHellefont, "Production of Thorium- and Plutonium-Diluted Sol-Gel Particles", *Sol-Gel Processes for Ceramic Nuclear Fuels*. Proc. of a panel on Sol-Gel Processes for Ceramic Nuclear Fuels, May 6-10, 1968, Vienna. International Atomic Energy Agency, 1968.
28. R. G. Wymer, "Laboratory and Engineering Studies of Sol-Gel Processes at Oak Ridge National Laboratory", *Sol-Gel Processes for Ceramic Nuclear Fuels*. Proc. of a panel on Sol-Gel Processes for Ceramic Nuclear Fuels, May 6-10, 1968, Vienna. International Atomic Energy Agency, 1968.
29. E. Zimmer and C. Ganguly, "Reprocessing and Refabrication of Thorium-Based Fuels", http://www.iaea.org/inis/aws/fnss/fulltext/0412_8.pdf Institut für chemische Technologie der nuklearen Entsorgung, Kernforschungsanlage Jülich GmbH (2005).
30. W. J. Lackey and T. L. Starr, "Fabrication of Fiber Reinforced Ceramic Composites by Chemical Vapor Infiltration: Processing, Structure and Properties." *Fiber Reinforced Ceramic Composites*. Ed. K.S. Mazdinyani. Park Ridge: Noyes Publications, 1990.
31. T. Tan, et al., "Simulation and Analysis for Melt Casting A Metallic Fuel Pin Incorporating Volatile Actinides", Proc. of the ASME International Mechanical Engineering Congress and Exposition, November 16-21, 2003, Washington, D.C.
32. G. Vandegrift, et al., "Lab-Scale Demonstration of the UREX+ Process." *Waste Management Conference*, Tucson, AZ February 29--March 4, 2004 (2004).
33. J. Law, et al., "Development and Demonstration of Solvent Extraction Processes for the Separation of Radionuclides from Acidic Radioactive Waste" *Waste Management* 19, 27 (1999).
34. M. Ozawa, et al., "A New Reprocessing System Composed of PUREX and TRUEX Processes for Total Separation of Long-Lived Radionuclides" *Fifth OECD/NEA Information Exchange Meeting on Actinide and Fission Product Partitioning and Transmutation*, SCK-CEN, Mol, Belgium; November 25-27, 1998 (1998).

35. C. de Oliveira and A. Goddard, "EVENT-A Multidimensional Finite Element-Spherical Harmonics Radiation Transport Code," Proc. Int. Seminar 3-D Deterministic Radiation Transport Codes, Paris, France, Organization for Economic Cooperation and Development (1996)
36. J.F. Briesmeister, Ed. "MCNP – A General Monte Carlo N-Particle Transport Code, Version 5," Los Alamos National Laboratory (2003).
37. "KENO V.a: An Improved Monte Carlo Criticality Program," NUREG/CR-0200, Rev. 7, Vol.II, Section F11, ORNL/NUREG/CSD-2/R7 (2004).
38. TRANSX 2" <http://t2.lanl.gov/codes/>
39. M. Kambe and M. Uotani, "Design and Development of Fast Breeder Reactor Passive Reactivity Control Systems: LEM and LIM", Nuclear Technology, 122, 179-195 (1998).
40. M. S. Kazimi and N. E. Todreas, *Nuclear Systems I: Thermal Hydraulics Fundamentals*, Hemisphere Publishing Corporation, New York pp 295-338 (1990).
41. E. Teughert, K. Haas, A. Van Heek, P. Kasten, "Distribution of the Decay Heat in Various Modular HTRs and Influence on Peak Fuel Temperatures," Energy Conversion Engineering Conference, Philadelphia, PA August 10-14, (1987).
42. M. S. Kazimi and N. E. Todreas, *Nuclear Systems I: Thermal Hydraulics Fundamentals*, Hemisphere Publishing Corporation, New York pp 16-17, 417, 684-5 (1990).
43. W. M. Stacey, *Fusion Plasma Physics*, Wiley-VCH Verlag GmbH & Co. KGaA, Weinheim (2005), ch 19.
44. J. Schlosser, F. Escourbiac, M. Merola, *et al.*, Nuclear Fusion **45**, 512 (2005).
45. ITER Technical Basis, Section 2.4, Divertor.
46. Fluent/Gambit, Version 6.1.22/s.1.2, "Computational Fluid Dynamics", Fluent Inc. (2004).
47. C.B. Baxi, C.P.C. Wong, Review of Helium Cooling for Fusion Reactor Applications, Fusion Engineering and Design **51-52**, 319-324 (2000).
48. F.P. Incropera and D.P. DeWitt, *Fundamentals of Heat and Mass Transfer*, 5th Ed., John Wiley & Sons, Hoboken, NJ (2002) Chapter 8.
49. B.R. Munson, D. F. Young, and T. H. Okiishi, *Fundamentals of Fluid Mechanics*, 4th Ed., John Wiley & Sons, Hoboken, NJ (2002) Chapter 8.

50. R. D. Stambaugh, "Future of Tokamak Facilities With a Burning Plasma Experiment", presentation to National Academies Burning Plasma Assessment Committee, 008-03/RDS/RS, January 18, 2003.
51. ITER Technical Basis, Chap. 2.5 Additional Heating and Current Drive, G A0 FDR 101-07-13 R1.0 (2001).
52. Y. Sakamoto, et al., "Stationary High Confinement Plasmas with Large Bootstrap Current Fraction in JT-60U", EX/4-3.
53. "Technical Parameters" Web Site <http://www.iter.org/index.htm>.
54. ITER Technical Basis, Chapter 2.1 Magnets, G A0 FDR 1 01-07-13 R1.0 (2001).
55. M. Huguet, "Key Engineering Features of the ITER-FEAT Magnet System and Implications for the R&D Programme" Nucl. Fusion, 41, 645 (2001).
56. "Triton: A Two-Dimensional Depletion Sequence for Characterization of Spent Nuclear Fuel," NUREG/CR-200, Rev. 7, Vol. I Section T1, ORNL/NUREG/CSD-2/R7 (2004).
57. N.F. Landers, L.M. Petrie, and D.F. Hollenbach, "CSAS: Control Module for Enhanced Criticality Safety Analysis Sequences," NUREG/CR-200, Rev. 7, Vol. 1 Section C4, ORNL/NUREG/CSD-2/V1/R7.

appendices

58. W. M. Stacey, *Fusion Plasma Physics*, Wiley-VCH Verlag GmbH & Co. KGaA, Weinheim (2005), ch 7.
59. "Focus On: JET Plasma Heating and Current Drive" Web Site <http://www.jet.efda.org/pages/focus/006heating/>.
60. ITER Physics Expert Group on Energetic Particles, Heating, and Current Drive, et al., "Chapter 6: Plasma auxiliary heating and current drive", Nucl. Fusion, 39, 2495-2539 (1999).
61. M. Porkolab, et al., "Electron Cyclotron Heating", Fusion Technology 1243-1249. Volume 21. May 1992.
62. G. Bosia, et al., "Phase II Proposal for the JET ITER-like IC H&CD Array", 9 June 2000.
63. D. W. Swain, et al., "FIRE Ion Cyclotron System Requirements and Design", ICRF Technology Workshop, Jackson Hole, Wyoming (5/21/2003).

64. K. Takahashi, et al., “Development of EC Launcher components for ITER”,
Journal of Physics: Conference Series 25 (2005) 75-83.